

# Probing Halos of Galaxies at Very Large Radii using Background QSOs<sup>1</sup>

S. Côté

*Canadian Gemini Office, Herzberg Institute of Astrophysics, National Research Council of Canada, 5071 West Saanich Road, Victoria, B.C., Canada, V9E 2E7*

Stephanie.Cote@nrc.ca

R. F. G. Wyse

*Department of Physics and Astronomy, Johns Hopkins University, 3400 N. Charles Street, Baltimore, MD 21218, USA*

wyse@pha.jhu.edu

C. Carignan

*Observatoire du Mont Mégantic et Département de Physique, Université de Montréal, CP 6128, Succ. centre ville, Montréal, H3C 3J7, Canada*

carignan@astro.umontreal.ca

K. C. Freeman

*Research School of Astronomy and Astrophysics, Mount Stromlo Observatory, ANU, Weston Creek ACT 2611, Australia*

kcf@msokcf.anu.edu.au

T. Broadhurst

*School of Physics and Astronomy, Tel-Aviv University, Tel-Aviv 69978, Israel*

tjb@wise.tau.ac.il

## ABSTRACT

Gaseous halos of nine nearby galaxies (with redshifts  $cz < 6000 \text{ km s}^{-1}$ ) were probed at large galactocentric radii using background quasars observed with HST GHRS and STIS. The projected quasar-galaxy separations range from 55 to  $387 h_{75}^{-1} \text{ kpc}$ .  $\text{Ly}\alpha$  absorption lines were successfully detected in the spectra

of five quasars, at impact parameters of up to  $\sim 170 h_{75}^{-1}$  kpc from the center of the nearby galaxy, and in each case at wavelengths consistent with the galaxy’s redshift. Our observations include the lowest redshift Ly $\alpha$  lines detected to date. HI velocity fields were obtained at the VLA for three of the galaxies in our sample (and in one case was available from the literature), to derive their rotation curves. When comparing the inner rotation curves of the galaxies with the velocity at large radius provided by the Ly $\alpha$  line it is apparent that it is very difficult to explain the observed Ly $\alpha$  velocity as due to gas in an extended rotating disk. In most cases one would need to invoke large warps in the outer gas disks and also thick gas disks in order to reconcile the observed velocities with the predicted ones. Indeed, in one case the Ly $\alpha$  line velocity indicates in fact counter-rotation with respect to the inner disk rotation. In light of these results we conclude that in a typical galaxy there is no longer detectable atomic gas corotating in an extended disk at radii  $> 35 \alpha^{-1}$ , where  $\alpha^{-1}$  is the stellar disk exponential scale-length. The cosmic web is the most likely origin for the detected Ly $\alpha$  lines. Our observations confirm the Bowen *et al.* (2002) correlation of equivalent widths with the local volume density of galaxies around the sightline, and the observed equivalent widths of the lines are consistent with expectations of the cosmic web.

*Subject headings:* galaxies: halos — galaxies: spiral — quasars: absorption lines — galaxies: ISM

## 1. Introduction

Rotation curves are the best tool to study the dark matter halos of galaxies, and the most extended ones will better constrain the dark matter halo parameters. Rotation curves derived from neutral hydrogen (HI) observations enable us to probe the dark matter potential to distances of at most 20 to 25  $\alpha^{-1}$  (where  $\alpha^{-1}$  is the optical disk exponential scale length), for gas-rich late-type spiral galaxies with particularly extended HI (eg. NGC2841 from Begeman 1987 or NGC2915 from Meurer *et al.* 1996). But it is not possible to obtain any kinematical data with 21cm emission further out than the radius at which the gas density falls to levels of a few times  $10^{19}$  atoms  $\text{cm}^{-2}$ , even with very sensitive observations, as the HI column falls off sharply beyond this point (eg. the ‘HI Edge’ observed in NGC3198, van

---

<sup>1</sup>Based on observations with the NASA/ESA Hubble Space Telescope, obtained at the Space Telescope Science Institute, which is operated by AURA, Inc. under NASA contract NAS5-26555.

Gorkom 1991). This sharp truncation of the HI distribution is believed to be the result of ionization of the atomic gas by the extragalactic UV radiation field (as predicted by Silk & Sunyaev 1976). At lower column densities the neutral fraction is therefore predicted to drop off dramatically in comparison to the total (ionized) hydrogen column (see Maloney 1993). Some studies have attempted to detect the faint ionized gas just beyond the HI limit from recombination emission in  $H\alpha$ . Depending on the volume density of the plasma at the critical column density where the outer disk becomes optically thin to this radiation (about  $N_{HI} \sim 3 \times 10^{19} \text{ cm}^{-2}$  for NGC3198), the emission measure from recombination radiation expected to be emitted by this ionized gas is only 0.025 to 0.25  $\text{cm}^{-6}\text{pc}$  (Maloney 1993). The only reported detection of recombination radiation so far is that of NGC253 for which sensitive Fabry-Perot observations by Bland-Hawthorn *et al.* (1997) managed to extend the HI rotation curve from 1.2 to 1.4  $R_{25}$ , with measured surface brightness values in  $H\alpha$  from 80 to 40 mR (millirayleighs, where 1 rayleigh =  $10^6/4\pi \text{ photons cm}^{-2}\text{s}^{-1}\text{sr}^{-1}$  or  $2.78 \text{ cm}^{-6}\text{pc}$  at  $H\alpha$ ). But at this level, as pointed out by the authors, the emission is probably not due to recombination after ionization by the metagalactic background, but rather from hot young stars near the center of the galaxy ionizing the warped outer HI disk.

If indeed spiral galaxies have extended (mostly ionized) gas disks it should then be possible to detect them in absorption in the spectrum of a bright background quasar, down to HI column densities of only  $\sim 10^{13} \text{ atoms cm}^{-2}$ . With such a suitably placed UV-bright background object one could obtain kinematical information on that galaxy's outer rotation curve out to 30 to 40  $\alpha^{-1}$  or more. At such radii the data could potentially reveal the extent of the dark matter halo, and constrain the mass profile out to such large galactocentric radii. This could then provide strong tests of cosmological galaxy formation scenarios. For example, according to the rotation curves predicted by Cold Dark Matter-dominated N-body simulations (e.g. Navarro, Frenk & White 1996) in low-mass dwarf galaxies we should detect a turn-down in the rotation curve if we could get data points just 15 or 20% further out in radius than currently mapped by HI observations. This matching of a  $\text{Ly}\alpha$  absorption line velocity with the kinematics of the nearest galaxy has already been attempted, originally by Barcons *et al.* (1995), who found that for two galaxies at  $z=0.075$  and  $0.09$  the  $\text{Ly}\alpha$  velocities as measured from background QSOs spectra at impact parameters  $64 h_{75}^{-1}\text{kpc}$  ( $= 16\alpha^{-1}$ ) and  $83 h_{75}^{-1}\text{kpc}$  ( $= 35\alpha^{-1}$ ), were consistent with gas in extended gaseous haloes co-rotating with the inner stellar disks (with  $h_{75}^{-1} = H_0/75$  where  $H_0$  is the Hubble constant and  $q_0 = 0$ ). On the other hand, Hoffman *et al.* (1998) found that the dwarf galaxy MCG+00-32-16, which is the closest galaxy to the low redshift  $\text{Ly}\alpha$  system in the sightline of 3C273, has an HI disk which would be counter-rotating compared to the  $\text{Ly}\alpha$  velocity. In this case however the impact parameter is 204 kpc which for the dwarf galaxy represents about  $153 \alpha^{-1}$ , in other words an excessively large radius to expect the extended gas halo to reach. More recently

Steidel *et al.* (2002) have obtained long-slit spectra of 5 intermediate redshift galaxies ( $0.44 \leq z \leq 0.66$ ) in the proximity of MgII absorbers sightlines (with projected separations from 19 to  $95 h_{75}^{-1} \text{kpc}$ ), and succeeded in reasonably matching the MgII absorbers' velocities with the galaxies' rotation curves, but only when setting various disk thicknesses and velocity scale heights (describing the velocity fall-off with  $z$ -height above the plane) case by case.

Our approach here is the reverse. Instead of identifying and analysing the galaxies found near the line-of-sight of a quasar exhibiting a known Ly $\alpha$  line, we start by selecting nearby galaxies, normal and well-behaved kinematically, hence easy to subsequently model dynamically, and search for bright background quasars at some particular impact parameter away, ie: at the interesting radii beyond the galaxy's HI envelope and up to about  $50 \alpha^{-1}$ . We then observe these quasars with HST, first to attempt to detect a Ly $\alpha$  line arising from the extended galaxy's disk, and then to use this Ly $\alpha$  line velocity to probe the outer dynamics of the galaxy.

Our study does not aim at elucidating the overall nature of all Ly $\alpha$  forest lines (other studies are better designed for this, by surveying all lines along several QSO sightlines and getting numerous spectra of galaxies in the surrounding fields eg. Penton *et al.* 2002, Morris *et al.* 2002). Indeed, while it is now generally accepted that most metal-line absorption systems found in QSO's spectra are associated with gaseous galaxy halos, the situation for the Ly $\alpha$  absorption systems has been long under debate. Some studies claim that (at least the stronger) Ly $\alpha$  lines are associated to extended halos of galaxies, while most believe that the majority of the lines occur in the intergalactic medium, tracing the 'cosmic web' (cf. van Gorkom *et al.* 1996), this intricate network of filaments and sheets of gas predicted by hydrodynamical simulations (eg. Davé *et al.* 1999). Some convincing arguments of the latter are the fact that several Ly $\alpha$  lines have been detected in voids (McLin *et al.* 2002), also confirmed by deep HI observations that would have detected dwarf galaxies and other low surface brightness galaxies (Shull *et al.* 1998). Also observations of double QSOs sightlines find Ly $\alpha$  lines in common in both spectra on scales of typically half a Mpc (Dinshaw *et al.* 1997, 1998). Here we are testing the simple conjecture that gaseous galactic disks extend further beyond that which can be probed in emission in HI, by searching for a corresponding Ly $\alpha$  line. More importantly, a successful detection, can be used as a dynamical probe of the outer halo of the galaxy.

In Section 2 we explain the selection of our targets, section 3 describes the observations (HST and radio), then section 4 discuss the results of matching the Ly $\alpha$  velocities with the galaxies' rotation curves and the implications.

## 2. Selection of Targets

Our list of QSO-galaxy pairs suitable for our purpose was compiled by cross-correlating all 646 quasars with  $V \leq 17.0$  in the Véron & Véron catalogue 6th edition (1993), with the *HI Catalog of Galaxies* (Hutchmeier & Richter 1989). This magnitude limit was imposed to make sure that the background QSO observations would stay within a reasonable amount of time to be feasible with HST. Our criteria for selection were:

i) the projected distance between the QSO and the galaxy was less than roughly 10 times the optical diameter ( $D_{25}$ ) of the galaxy. This was to find QSOs in the interesting region beyond the galaxy’s HI emission extent but where the column density of neutral gas would still be high enough to be detected in absorption (assuming that galaxies have extended gaseous disks out to large radii as suggested by eg. Chen *et al.* 2001).

ii) the galaxy systemic velocity was  $\geq 550 \text{ km s}^{-1}$ . This ensured that the associated Ly $\alpha$  detection stayed clear from the Geocoronal Lyman- $\alpha$  emission at 1216 Å (from the Earth’s exosphere). Moreover this also ensured that the Ly $\alpha$  detection’s velocity would not fall in the range covered by the damped Ly $\alpha$  wing of our Galaxy, which can extend to  $\simeq 1220 \text{ Å}$  towards some sightlines, depending on the total HI column density present in that direction. If a galaxy’s systemic velocity is too low, any associated line would get lost in the wing of the Galactic damped line, where the continuum against which to detect this absorption line is seriously depleted.

iii) the galaxy was not interacting and was relatively isolated. This means that an observed Ly $\alpha$  line would be fairly unambiguously assigned to that object, ie: QSO-galaxy pairs in the middle of clusters, such as for 3C273, were discarded (but one target, NGC5033, was later found to be surrounded by several dwarf galaxies, see Section 4.1).

iv) the galaxy’s optical diameter was at least  $\geq 1'$  so that a detailed kinematical study, using HI rotation curves, is feasible (since the HI radio beams will be in the best cases about a dozen of arcsecs). In some cases the rotation curves were already available in the literature. For the same reason the galaxy also had to appear “well-behaved”, with no obvious distortions or morphological asymmetries – in other words as normal as possible.

We observed a sample of 9 QSO-galaxy pairs with HST, chosen to cover a range of morphological types (Sa to Sd), with a range of magnitudes  $-20 < M_B < -15.1$ . Assuming successful detections of Ly $\alpha$  absorption lines, this would allow testing of scaling relations across a wide range of galaxy properties. For example Chen *et al.* (1998), in their study of 26 galaxy-absorber pairs with separations ranging from 16 to  $209 h_{75}^{-1} \text{ kpc}$ , find that the strength of the absorption depends not only on the impact parameter separation but also on the B-band luminosity of the galaxy. Hence galaxies with a wide range of properties were

chosen for our sample to investigate these possible trends. Table 2 lists the properties of our selected target galaxies. Note that the impact parameters of the galaxy-QSOs are based on distances estimated using  $H_0 = 75$  km/s/Mpc. In the case of NGC2841 there is a Cepheid distance of  $14.1 \pm 1.5$  Mpc (Macri *et al.* 2001). Its velocity simply estimated with  $H_0 = 75$  would give a distance of 8.5 Mpc, which is only 60% of this ‘true’ distance. Hence this gives an idea of the possible large uncertainties in these impact parameters estimates.

### 3. Observations and Reductions

#### 3.1. HST Observations of QSOs

Spectroscopy of our 9 target QSOs was obtained with the HST GHRS through the Small Science Aperture (SSA) with the G140L grating, as well as with the HST STIS/FUV-MAMA through the 52X0.1 aperture with the G140L and G140M gratings, as listed in Table 1. This Table also gives details of the observations (the HST dataset filenames, date of the observations) and the total integration times of the spectra. Since the QSOs have a range of fluxes, the integrations were set such as to result in a  $3\sigma$  limiting equivalent width of at least  $0.3 \text{ \AA}$ , or in the case of the STIS data, to fill completely the one orbit necessary (this  $3\sigma$  limit being in almost all cases achievable in less than one orbit).

The preliminary GHRS data reduction was carried out with the standard CALHRS software using the final GHRS reference files, and further reduction and analysis were performed with the IRAF/STSDAS package. To fully sample the PSF, quarter-diode substepping was employed, producing four spectra per exposure. With this mode 6% of the time is spent measuring the background with the science diodes. The wavelength shifts between these different groups, and then between the different exposures, were determined to align all the spectra before combining them and merging the wavelength and flux information. With the G140L grating the dispersion is  $0.57 \text{ \AA}$  per diode, corresponding to a velocity resolution of about  $140 \text{ km s}^{-1}$  at  $1200 \text{ \AA}$ . The default wavelength scale is expected to have a maximum rms of  $55 \text{ m\AA}$  for G140L. However, zero-point shifts can be significant: even though we used the small aperture which will limit the effect of the uncertainty in the position of the target within the aperture, thermal effects in the GHRS as well as geomagnetic effects are a large source of wavelength error (see GHRS Instrument Handbook). The wavelength accuracy achievable is about  $30 \text{ km s}^{-1}$ , even when a wavelength calibration exposure is obtained just before the science exposure. For this reason these zero-points were corrected by assuming that low-ionization Galactic interstellar lines lie at the same velocity as the observed dominant component of the Galactic HI along these sightlines. The strongest Galactic lines were used such as Si III  $\lambda 1206.5$ , Si II  $\lambda 1260.4$  and CII  $\lambda 1334.5$ . The Galactic HI LSR velocity

measurements were taken from the Leiden/Dwingeloo survey (Hartmann & Burton 1997).

For the STIS observations, the G140M centered at 1222 Å provides a resolution of 20 km s<sup>−1</sup> (with a pixel size of 0.05 Å) and wavelength coverage from 1195 to 1249 Å. In addition short G140L observations were obtained for the 3 QSOs at higher redshifts (PG1049-005, PKS1103-006, and PG1259+593). This was to make sure that any absorption feature detected at 1218-1222 Å (where our Lyα lines are expected) is not in fact a Lyβ line associated with some Lyα line at higher redshift along the sightline. The G140L therefore provided us with a spectrum over a larger wavelength range (roughly 1130 to 1720 Å) to check on this possibility. The standard CALSTIS procedures were followed to flatfield the individual spectra, extract them and then wavelength-calibrate and flux-calibrate them. The MAMA spectroscopic accuracy is expected to be about 0.2 pixel when using the narrow slit (<3 km s<sup>−1</sup> with G140M), but is ill-defined in practice. Hence the zero-points were corrected the same way as for the GHRS data, by shifting Galactic lines in the spectra to the main Galactic HI LSR velocity. In this case the Galactic lines used were Si III λ1206.5 and NI λ1199.55, λ1200.22, λ1200.71 when suitable. For the Galactic HI velocities, several sightlines had higher resolution HI Galactic spectra from Effelsberg (Wakker *et al.* 2001, 9'.1 beam), and for the rest the measurements were extracted from the Leiden/Dwingeloo survey (Hartmann & Burton 1997, 36' beam), or from NRAO 43m data (Lockman & Savage 1995, 21' beam). Care was taken with galactic features at non-LSR velocities due to High-Velocity Clouds (HVCs) present in some of our sightlines. For example the MRK876 sightline crosses the region of Complex C, a prominent HVC covering 10% of the northern sky, and consequently the Galactic and Complex C Si III line are blended in the spectrum (Gibson *et al.* 2001). Our final shifts applied to the spectra differed from the original calibration by 0.8 km s<sup>−1</sup> up to 11.6 km s<sup>−1</sup> at most. Finally, after continuum fitting and normalization with a low-order polynomial, wavelengths and equivalent widths were measured, and Voigt profiles were fitted to the observed absorption lines. These profile fits are depicted in Figure 3. In the case of PG1309+355, slightly better residuals were obtained if fitting 3 subcomponents to the line, and similarly for PG0804+761 with 2 subcomponents. For sightlines with non-detections, equivalent width limits were calculated following the equations of Ebbets (1995).

Lyα absorption lines were successfully detected for 5 of our QSO-galaxy targets (illustrated in Figure 1). Figure 2 shows the (unbinned) spectra with the detections, as well as the 4 spectra with non-detections. Table 2 lists the detections, and their corresponding velocities and equivalent widths. In many cases other Lyα lines were also detected along the same sightlines at other various redshifts, and do not necessarily seem to be associated with any nearby galaxy. These will be discussed more fully in a forthcoming paper. In all cases the velocities of our detections agreed within errors with those in the literature when available, for example from higher resolution FUSE data detecting the Lyβ counterparts of

some of our lines. For PG0804+761 our line of interest at  $V_{Ly\alpha}=1570\text{ km s}^{-1}$  has not been previously reported, but a higher redshift line in the spectrum which we detect at  $V_{LSR}=5561 \pm 8\text{ km s}^{-1}$  has been reported by Shull *et al.* (2000) at  $V_{LSR}=5565\text{ km s}^{-1}$  and by Richter *et al.* (2001) at  $V_{LSR}=5553\text{ km s}^{-1}$  (from a FUSE Ly $\beta$  line). For MRK876 Shull *et al.* (2000) report a  $V_{LSR}=958\text{ km s}^{-1}$  (no errors quoted) for which we have  $V_{LSR}=950 \pm 5\text{ km s}^{-1}$ .

For the equivalent widths, a large part of the uncertainties come from the continuum fitting, especially since some of the lines are sitting on the edge of the Galaxy’s Ly $\alpha$  damped wing. Hence the errors as presented in Table 2 are the sums in quadrature of the uncertainties ( $1\sigma$ ) from photon noise and the estimated errors from different reasonable placements of the continuum fit. The continuum Signal-to-Noise per resolution element in our spectra in the region of the expected or detected absorption ranges from 2.2 to 12, since our target QSOs have a wide range of fluxes (the lowest S/N of 2.2 is for PKS1103-009 which had a detected flux of only 3/5 of the value estimated from IUE data).

### 3.2. HI Observations and rotation curves

To compare the five detections of Ly $\alpha$  absorptions in spectra of background QSOs with the associated galaxy’s kinematics we needed its velocity field and rotation curve. For NGC5033 and UGC8146 these were available in the literature (Begeman 1987; Rhee & van Albada 1996). For the other 3 galaxies we carried out Very Large Array (VLA) HI observations, for which the observational parameters are summarized in Table 3. The correlator was set to a 3.125 MHz bandwidth with 128 channels, for a channel separation of  $5.2\text{ km s}^{-1}$ . The calibration and reductions were performed with the NRAO package AIPS, following standard procedures. The absolute flux calibration was determined by observing the standard source 1331+305. After applying calibration and bandpass corrections to the *uv* databases, the continuum emission was subtracted in the visibility domain using channels free of line emission. Several sets of maps were produced for each galaxy, one with uniform weighting preserving the best resolution, and a few with natural weighting smoothed to various larger beams. These sets of maps were CLEANed well into the noise by monitoring the total cleaned flux as a function of the total number of CLEAN components recovered, and finally were restored with a circular symmetric Gaussian beam. These maps were then corrected for the beam response of the antennae to rectify for attenuation away from the center of the primary beam. No HI emission was detected from other galaxies within the primary beam and through the bandwidth observed other than the intended source.

Moment maps were obtained from each datacube using Hanning smoothing in velocity and Gaussian smoothing spatially, to produce integrated total HI column density maps,



intensity-weighted velocity maps, and velocity dispersion maps. HI rotation curves were obtained by fitting a tilted-ring model to the velocity fields (Begeman 1987, Côté *et al.* 2000), and are given in Table 4. In each case the rotation curves are slowly rising and just barely reach the flat part at the last measured points. The errors in velocity were calculated from half the difference between the velocities on each side (receding and approaching) or from the formal errors given by the least-squares fits, whichever were the highest. The rotation curves were derived with the systemic velocities and orientation parameters (position angle and inclination) set to the values shown in Table 3. The derived systemic velocities agree extremely well with the RC3 values, within  $1 \text{ km s}^{-1}$ . The orientation parameters as well agree within a few degrees with those derived optically (from the RC3), which show that these galaxies do not have strong warps in their outer HI gaseous envelopes. The HI distributions and HI velocity fields are shown in Figure 4, and the gas surface density profiles in Figure 5, for which the HI surface density values were scaled by 4/3 to account for the presence of helium. Although the three surface density profiles differ greatly, they are all within the range of what is commonly detected in late-type spirals.

## 4. Results

### 4.1. $\text{Ly}\alpha$ detections

Figure 2 show the 5  $\text{Ly}\alpha$  absorption detections amongst our 9 target QSOs, and Table 2 gives their details. The target galaxy-QSOs which give rise successfully to a  $\text{Ly}\alpha$  detections have impact parameters from 55 kpc to  $169 h_{75}^{-1}$  kpc, and the detections correspond to HI column densities ranging from  $\log N_{\text{HI}}=13.0$  to  $13.9 \text{ cm}^{-2}$ . PG1309+355-NGC5033 with an impact parameter of  $276 h_{75}^{-1}$  kpc, also give rise to a detection, however in this case it was later found that NGC5033 is part of a small loose group of galaxies and is surrounded by a swarm of dwarf galaxies, some of which are closer to the QSO sightline than is NGC5033 (eg., UGC8261, UGC8323, UGC8314); and it is hence not possible to attribute the absorption detection to NGC5033 alone. We will return to this case later on.

In each case the  $\text{Ly}\alpha$  line velocity matches extremely well the systemic center-of-mass velocities of the galaxies. In particular for PG 1259+593 and MRK 876 their  $\text{Ly}\alpha$  absorption lines correspond to velocities of 679 and  $935 \text{ km s}^{-1}$  (respectively), which are the lowest redshift  $\text{Ly}\alpha$  lines ever detected so far in association with nearby galaxies. Presumably closer galaxies, e.g. M31, could produce  $\text{Ly}\alpha$  lines of even lower redshift but they would be impractical to detect because of the damped wing of the Milky Way Galaxy absorbing away all the continuum flux. In fact in Figure 2, in all our spectra, the slope of the Galaxy’s damped wing is clearly seen, ie: the  $\text{Ly}\alpha$  detections are sitting inside the range covered by

the Galaxy’s damped wing which extends to at least  $\sim 1220 \text{ \AA}$ , sometimes  $1222 \text{ \AA}$ .

As for the  $\text{Ly}\alpha$  non-detections, they occur for galaxy-QSO separations ranging from 162 to  $387 h_{75}^{-1} \text{ kpc}$ . Their  $3\sigma$  limiting equivalent width is in each case above the level needed to detect an absorption line even weaker than the ones detected in the other five spectra. In terms of HI column density limits it corresponds to a  $3\sigma$  detection limit around  $\log N_{\text{HI}}=13.1 \text{ cm}^{-2}$  on average. This at first sight thus appears to confirm the findings of several studies of moderately low redshift galaxy surveys associated with absorbers, which seem to point to most galaxies being surrounded by tenuous gas out to  $\sim 240 h_{75}^{-1} \text{ kpc}$ . Chen *et al.* (1998) and (2001), in a continuation of the work of Lanzetta *et al.* (1995), find for 34 galaxies and absorbers pairs at  $z=0.07$  to  $0.89$  with impact parameters  $\rho$  from roughly 16 to  $233 h_{75}^{-1} \text{ kpc}$ , a near unity covering factor for tenuous gas halos around typical  $L_*$  galaxies out to a radius of  $\sim 240 h_{75}^{-1} \text{ kpc}$ . Furthermore Chen *et al.* (1998) found that the absorbing gas equivalent width depends on the galaxy-QSO impact parameter as well as the galaxy B-band luminosity, which if true would greatly strengthen the case for a direct association between the absorber and its nearest galaxy. Meanwhile Bowen *et al.* (1996) found that for 38 galaxies at  $z=0$  to  $0.08$  lying at  $< 400 h_{75}^{-1} \text{ kpc}$  from a sightline of a bright QSO observable with FOS, for lines with equivalent widths  $> 0.3 \text{ \AA}$  the covering factor is 44% between 67 to  $400 h_{75}^{-1} \text{ kpc}$ . Recently Bowen *et al.* (2002) detected  $\text{Ly}\alpha$  lines in the outer regions of all eight nearby galaxies probed, with impact parameters up to  $265 h_{75}^{-1} \text{ kpc}$ , down to  $W > 0.1 \text{ \AA}$ . Our results concord with these studies. All of our detections occur at impact parameter  $< 180 h_{75}^{-1} \text{ kpc}$  from the nearest galaxy, and only one of our non-detections occurs for  $\rho < 180 h_{75}^{-1} \text{ kpc}$  (PKS1103-006 - NGC3521 at  $\rho=162 h_{75}^{-1} \text{ kpc}$ ). Note however that there is considerable uncertainty in the values of  $\rho$  due to the distance dependence (see above). All these results seem very suggestive of a link between the detected absorbers and their neighboring galaxies. But one needs to look into the detailed kinematical match between the  $\text{Ly}\alpha$  absorption line and the kinematics of the inner galaxy to probe more directly any direct link between an extended gaseous disk or halo of the galaxy and the absorber’s velocity.

#### 4.2. Matching the galaxies’ kinematics with the absorbers

We will try to compare here the velocity of the QSO  $\text{Ly}\alpha$  system, with that of the associated galaxy. For 4 out of 5 detections, the associated galaxy is confirmed to be isolated, hence the absorber can be unambiguously matched to this galaxy, assuming it is indeed due to a galaxy. For 3 of these galaxies, UGC4238, UGC7697 and NGC6140, we obtained the HI rotation curves (section 3). The 4th one, UGC8146, has been observed by the Westerbork Synthesis Radio Telescope and its rotation curve was extracted from Rhee & van Albada

(1996).

To compare the inner galaxy dynamics with the velocity measured by the Ly $\alpha$  line, we will assume that the line does indeed arise in the extended gaseous disk of the galaxy and see how well it matches the velocities of the HI rotation curve in that case. The observed radial velocity of the line,  $V_{obs}$ , is related to the corresponding rotation velocity  $V_{rot}$  in the disk of the galaxy by:

$$V_{obs} = V_{sys} + V_{rot}\sin(i)\cos(\theta) \quad (1)$$

where  $V_{sys}$  is the systemic velocity of the galaxy,  $i$  is its inclination, and

$$\cos(\theta) = \frac{X}{R} \quad (2)$$

where the QSO has coordinates, in the plane of the sky, of X along the galaxy major axis, and Y along the minor axis, with

$$R = \sqrt{X^2 + Y^2\sec^2(i)} \quad (3)$$

R is the radius in the plane of the galaxy at which the measurement lies, in other words, the deprojected impact parameter of the QSO (a figure demonstrating these formulae is provided in Kerr & de Vaucouleurs 1955, in which however the inclination angle is defined as  $i=0$  for an edge-on galaxy contrary to the modern convention). For the orientation parameters of our galaxies we have used those derived from the fits to their HI velocity fields.

Figure 6 shows the resulting rotation curves. The inner points show the velocities obtained from the HI velocity fields, and the single outer point is from the Ly $\alpha$  detection. The plotted curves are simply the best fits CDM models (Navarro, Frenk & White 1996) to the inner rotation curve, and serve to guide the eyes to what velocities might be expected in these outer parts (note that such CDM curves are actually bad fits to observed rotation curves in the inner parts, see, e.g. Côté *et al.* 2000, but here we just need them as rough approximations for the outer parts). The rotation curves in every case just reach the flat part at the very last measured point(s) (see Table 4). Each case is discussed separately below.

#### 4.2.1. NGC 6140

NGC 6140 is the only galaxy for which the Ly $\alpha$  velocity could be reasonably reconciled with the value expected if indeed arising from an extended gaseous corotating disk. Although the Ly $\alpha$  line velocity is much lower than the maximum rotation velocity  $V_{max}$  of the inner rotation curve, or than the velocity expected from CDM models at that radius, there are some ways to make it consistent with a disk velocity at that radius. For example a strong warp in

the orientation parameters of the galaxy in the outer parts would change the deprojection factors and hence the calculated Ly $\alpha$  rotation velocity could rise to match the expected value. The present Ly $\alpha$  velocity was calculated using the HI orientation parameters. One would need a warp as large as about 40° in inclination, or alternatively of 22° in inclination and -31° in position angle, to bring the velocity in line with the disk expected one. Most galaxies are observed to be warped in their outer parts, but such strong warps are rare for isolated galaxies. But although unusually large, one cannot a priori dismiss the possibility of such a warp in NGC6140. Another possibility to consider is if the disk, and the dark matter halo as well, of NGC6140 are truncated -for whatever reasons- just outside the radius of the last measured point in HI. In this case the velocities in the outer parts should follow a keplerian fall-off, and the velocity expected at the radius of the Ly $\alpha$  velocity would fall to about 46.2 km s<sup>-1</sup>, close to the measured  $V_{Ly\alpha}=36.2 \pm 5$  km s<sup>-1</sup>. Finally another possibility is that the velocity measured is not due to gas actually in the disk plane, but from material at a certain  $z$  height in a thick disk or halo. Assuming a thick rotating disk in which the circular velocities decrease rapidly as a function of scale height,  $v(z) = v_d e^{-|z|/h}$ , where  $v_d$  is the velocity in the disk midplane and  $h$  is a velocity scale height, then one can easily recover from the model a lower velocity like the one observed here by choosing an appropriate value of  $h$ . Except in the case of an infinitely large  $h$  where the thick disk is corotating cylindrically, the velocities at some  $z$  distance will be much lower than the midplane one. This is observed in NGC 891 for example, in which some HI halo gas extending up to 5 kpc from the plane is seen to rotate 25 to 100 km s<sup>-1</sup> more slowly than the gas in the plane (Swaters, Sancisi & van der Hulst 1997). Hence the observed Ly $\alpha$  velocity of NGC6140 would not be at all unphysical but would simply reflect the presence of a rotating thick disk (with detectable gas only at higher  $z$  height, and none in the plane of the disk). For the moment, with only one sightline velocity at large radius, it is not possible to discriminate between these various possibilities and confirm any of them.

#### 4.2.2. UGC4238 and UGC8146

The situation for UGC4238 and UGC8146 is different. In these two cases, assuming planar kinematics, the measured Ly $\alpha$  velocity corresponds to a circular velocity actually larger than the expected CDM one or even the  $V_{max}$  reached by the inner rotation curve. A very significant increase of rotation velocity with radius would be required to explain the observed velocity. However one can again invoke warps to make the observed velocity consistent with the extrapolation of the inner disk rotation. In fact in these two cases, because of the particular orientation parameters of the galaxies and their angle with respect to their associated quasars' sightline, one would need only mild warps (of the order of 10° in

the suitable direction) to make the match. Consequently one can still not dismiss a priori the possibility that the absorptions indeed arise from co-rotating gaseous extensions of the inner disks, albeit non-planar motions.

#### 4.2.3. UGC7697

The QSO, TON1542, is situated at the South-West of the galaxy; the observed velocity ( $V_{obs} = 2557 \text{ km s}^{-1}$ ) is greater than the systemic velocity ( $V_{sys}=2536$ ); yet the galaxy’s approaching side is towards the West, meaning the velocities should all be smaller than  $V_{sys}$ . The observed velocity from the absorption line is counter-rotating with respect to the disk velocities. And the observed velocities and geometry of the case of UGC7697 are such that warps cannot provide consistency with an extended gas disk. Unusually large warps would be required to reverse the inclination of the disk on the sky so that counter-rotation is observed, and such twisted rotating disks would be unlikely to be stable (with the exception of nearly face-on galaxies where the reversal of the inclination would be easier to achieve; see for example Cohen 1979 or Appleton, Foster & Davies 1986, where such a possibility is discussed to explain the apparent velocity reversals in IC10 and M51). Counter-rotation at very large radii has been observed in HI in a few galaxies, but those are always galaxies interacting with a nearby dwarf (for example NGC4449, Hunter *et al.* 1998) or which also harbour inner counter-rotation and hence easily stand out morphologically (like NGC4826, the ‘Evil-Eye’ galaxy, Braun *et al.* 1994). Neither of these cases apply here for any of the galaxies in our sample. In the case of UGC7697 no amount of disk thickening, or warps could explain the discrepancy (unless abnormally large). There are simply no physical way to produce such a velocity with an extended corotating disk. This is sobering because UGC7697 is one of the galaxies for which the QSO is at the smallest impact parameter, and yet the absorption’s velocity does not match. It is also interesting to note from Figure 1 that for UGC7697 the QSO lies close to the projected optical major axis in angle (compared to the other galaxies). If the gas has a higher column density in the disk than in the halo we should have expected a clear detection of the rotating HI disk of UGC7697, if it does reach out to this radius at the  $N_{HI} = 10^{13} \text{ cm}^{-2}$  level.

Note that some have invoked the existence of very low-surface brightness galaxies or dwarf galaxies, undetected in the optical, which could lie closer to the QSO sightline than the apparently nearest galaxy and from which the  $\text{Ly}\alpha$  line would originate. In the case of UGC7697 this is very unlikely since we also acquired deep HI pointings with the VLA on all of our QSOs fields and should have detected such galaxies, down to a few  $10^6 M_{\odot}$  (to be presented in a forthcoming paper).

#### 4.2.4. From the literature: NGC988 and NGC3942

Our conclusion that the Ly $\alpha$  absorptions cannot arise in simple extended disks are confirmed by two other galaxies associated with Ly $\alpha$  absorbers taken from the literature, for which similar results are found. Bowen, Pettini, and Blades (2002) targeted a sample of eight nearby galaxies near the sightlines of QSOs and AGNs. Most of their galaxies are not isolated (contrasting with the careful selection criteria of our sample), but are part of binary pairs or small groups (their sample was produced by cross-correlating the RC3 with the Veron-Cetty & Veron (1996) catalog, and choosing galaxies with  $> 1300 \text{ km s}^{-1}$ , and with impact parameters to QSOs of less than  $200 h_{100}^{-1} \text{ kpc}$ ). However two galaxies, NGC988 and NGC3942 are reasonably isolated, at least on the scale of a few hundreds of kpc. Their projected separations from their associated QSOs are 211 and  $123 h_{75}^{-1} \text{ kpc}$  respectively, and no other galaxies are known around a diameter of 400 kpc from these QSO sightlines. Unfortunately no rotation curves, either optical (in H $\alpha$ ) or HI, are available for these two galaxies. But for the sake of comparing the inner galaxy’s kinematics with the Ly $\alpha$  absorption velocity, we can use NGC988 and NGC3942’s magnitude to derive approximate rotation curves, using the ‘universal rotation curve’ of Persic & Salucci (1996) (where they obtained, based on a sample of 1100 rotation curves, a relation between the shape and amplitude of a rotation curve, and the luminosity of the galaxy). We will see below that these approximations are more than satisfactory to be able to draw our conclusions. The Ly $\alpha$  line velocities observed in the spectra of MRK1048 and PG1149-110 respectively are taken from Bowen *et al.* (2002). One last important piece of information needed to compare the inner and outer velocities is that the sense of rotation of the galaxy must be known, ie. we must determine if the QSO lies behind the approaching or the receding side of the galaxy (otherwise it is not known if the velocity difference is due to corotation or counter-rotation). This might be difficult to establish without a proper 2D velocity field for these two galaxies. Fortunately NGC988 and NGC3942 are reasonably nearby and extended in angular size, and hence their HI envelope should be at least a few arcmins in diameter. In that case it is possible to detect the change in shape of the HI global profile at different positions around the galaxy in the HIPASS scans (HIPASS is the All-Southern-Sky HI survey performed with the Parkes Multibeam receiver and available on-line, Barnes *et al.* 2001). By retrieving the HI profiles on each side of the galaxy (the pointings in the on-line catalog are separated by roughly 8 arcmins from each other), it is possible to follow the change from a double-peak profile for NGC988 (with a systemic velocity of  $1504 \text{ km s}^{-1}$ ) to a single peak roughly at  $1400 \text{ km s}^{-1}$  at the East to one around  $1600 \text{ km s}^{-1}$  at the West, and hence determine that for NGC988 the approaching side is at the East and the receding one at the West. Similarly for NGC3942 the approaching side is seen to be in the South-East and the receding one in the NorthWest. With this information one can then plot the rotation curves of Figure 7. They

confirm the findings on our galaxies above. Because for NGC988 the velocity difference between the Ly $\alpha$  absorption line and the systemic velocity of the galaxy is already quite large, this translates into a rotation velocity (with the appropriate deprojections) which is ridiculously too elevated ( $\sim 1192 \text{ km s}^{-1}$ ), and no amount of warping, no matter how severe, can bring this velocity down to a value close to  $V_{max}$ . For NGC3942 the calculated rotation velocity is also inadequate, as we find here another case of counter-rotation. Again NGC3942 has a relatively small impact parameter to the Ly $\alpha$  line, compared to those in our sample, with the projected distance corresponding to  $147 h_{75}^{-1} \text{ kpc}$ , and yet already at that radius we do not detect any longer the extended corotating gaseous disk of the galaxy.

### 4.3. The nature of the Ly $\alpha$ detections

Could it be that somehow, although not in a corotating disk or halo, this detected gas is still associated to the galaxy? After all the Milky Way is known to be surrounded by High-Velocity-Clouds, which can have velocities above, or below, the Galaxy’s rotation velocity by several hundred  $\text{km s}^{-1}$  (see, e.g. Wakker 1991). Following strong supernovae events some ejected gas might hide into a hot phase until eventually it cools down and could then be detected to low column densities in our sightlines at very large radii. Multiple supernovae remnants can drive a superbubble evolving quickly into a blowout, leaving a hole in the galactic disk (eg. MacLow & McCray 1988). Some gas can even be accelerated beyond the escape velocity and be ‘blown-away’, completely unbound from the galactic potential (de Young & Heckman 1994). For small dwarf galaxies, for which it is easier to escape the potential, it might be possible to generate large (100 kpc size) gaseous halos with supernovae-driven winds (Nath & Trentham 1997). For larger galaxies it is expected that there should be a local circulation of gas (to a few scalelengths above the disk) via a fountain-type flow (Shapiro & Field 1976). However it might be unlikely though to blow gas out of a more normal galaxy (closer to  $L_*$ ) to distances of more than 100 kpc, corresponding to factors of up to 7.5 times the diameter of the galaxy -as is the case here for NGC6140.

Another possibility is that we are intercepting satellites objects (very small galaxies or clouds of gas) orbiting around the primary galaxy. This would explain the counter-rotating velocities, as satellite objects can have retrograde as well as prograde orbits. In fact in the study of the supermassive disk galaxy NGC5084 orbited by a record number of 9 satellite dwarf galaxies (Carignan *et al.* 1997), the large majority of the satellite objects (7 out of 9) are on retrograde orbits. The problem with this explanation though is the overly large covering factor of the detected gas for impact parameters  $< 160 \text{ kpc}$ . In the Bowen *et al.* (2002) study they find a detection for *all* QSOs at impact parameters  $< 265 h_{75}^{-1} \text{ kpc}$  (down to  $W >$

0.11 Å), and in our case all QSOs at  $< 136 h_{75}^{-1}$  kpc yield a detection. It would thus be very unlikely that by chance the sightlines always intercept one of the satellites, considering especially the range of orientation parameters of the targets. Moreover these satellite objects would have to have very unusual properties compared to other dwarf galaxies, since we have deep VLA HI pointings of all our fields in which we would have detected any objects above about  $10^6 M_{\odot}$  (to be presented elsewhere).

Another important clue in constraining the nature of the detected Ly $\alpha$  absorbers is the inspection of the lines' equivalent widths. A strong argument in favour of the extended galactic disks' origin of the Ly $\alpha$  lines has been the apparent anti-correlation between equivalent width and impact parameter for the lines, the absorption being stronger the closer it is to the galaxy (Lanzetta *et al.* 1995). The Chen *et al.* (1998) study find also a dependence on the luminosity of the galaxy, of the form:

$$\log\left(\frac{N}{10^{20} \text{cm}^{-2}}\right) = -5.33 \log\left(\frac{\rho}{10 \text{kpc}}\right) + 2.19 \log\left(\frac{L_B}{L_{B*}}\right) + 1.09 \quad (4)$$

meaning that brighter galaxies would have stronger absorptions at a given radius. Tripp *et al.* (1998) discussed a few possible selection biases that could explain this anti-correlation. Most interestingly Bowen *et al.* (2002) plotted this relation for their 8 nearby galaxy-QSO pairs and found that the Chen *et al.* luminosity dependence is not confirmed. In fact they found a correlation in the *opposite* sense, significant at the  $2.8\sigma$  level, implying that stronger absorbing lines are associated with fainter galaxies. They concluded that this relation is probably coincidental, simply a result of small number statistics. In our data, with four points, we find a dependence in-between that of Chen *et al.* (1998) and Bowen *et al.* (2002), in fact it is consistent with no dependence on luminosity. Meanwhile the hydrodynamical simulations of Davé *et al.* (1999) have been able to successfully reproduce the anti-correlation of equivalent widths and impact parameters in the context of the cosmic web. They showed that the cosmic gas which loosely trace the large scale structure will have 3 phases: the strongest absorbers arise near galaxies because the gas is denser there; the majority of the absorbers will arise at impact parameters between 40 and  $360 h_{75}^{-1}$  kpc from shock-heated gas around galaxies; and at impact parameters further than  $360 h_{75}^{-1}$  kpc the absorbers will be associated with a cooler diffuse gas component.

This is corroborated by another interesting correlation, plotted by Bowen *et al.* (2002), between the equivalent widths and the local volume density of galaxies. For each of the sightlines they calculated the total equivalent width by summing all lines within  $\pm 500$   $\text{km s}^{-1}$ , and plotted them against the number of galaxies with  $M_{lim} < -17.5$  in a cylinder of  $2 h^{-1}$  Mpc radius with a length equal to the distance between  $+500 \text{ km s}^{-1}$  and  $-500 \text{ km s}^{-1}$  from the Ly $\alpha$  line. Their choice of  $M_{lim}$  was dictated by the limiting apparent magnitude for completeness in the RC3 along their sightlines. They find that the higher the



density of  $M_B < -17.5$  galaxies in a given volume, the stronger the equivalent width of Ly $\alpha$  absorption over  $1000 \text{ km s}^{-1}$ . This suggests that the strength of the Ly $\alpha$  absorbers are not related to their nearest galaxy neighbour but rather to the overall volume density of galaxies within a few Mpc of the sightline.

In Figure 8 is plotted similarly our Ly $\alpha$  lines versus the estimated volume density of galaxies around our targets. Following Bowen *et al.* (2002) we summed all components of Ly $\alpha$  absorption within  $+500 \text{ km s}^{-1}$  and  $-500 \text{ km s}^{-1}$  from the main Ly $\alpha$  line. Only in one case (PG0804+761) was there another Ly $\alpha$  absorber to add up within that range. We considered similarly only galaxies with  $M_{lim} < -17.5$  within a  $2 h^{-1}$  Mpc radius and within  $+500 \text{ km s}^{-1}$  and  $-500 \text{ km s}^{-1}$  in the RC3.

Our data agree very well with the Bowen *et al.* (2002) result, within errors (our errors in  $n$  are simply  $\sqrt{n}$ ). The sightline to TON1542 goes through the least dense area (with only 2 bright enough galaxies within the  $2 h^{-1}$  Mpc radius) and the Ly $\alpha$  line is indeed the weakest of all our targets. On the other hand, the sightline to PG1309+355 and close to NGC5033 is surrounded by galaxies (in fact we had to a posteriori eliminate NGC5033 from the rotation curve analysis precisely because of this, there are too many other galaxies close to the QSO and hence it was not possible to attribute the Ly $\alpha$  detection to a galaxy in particular). And the Ly $\alpha$  line in the spectrum of PG1309+355 is by far the strongest and most complex, blending several components into a line with total equivalent width of  $1.14 \pm 0.09 \text{ \AA}$ . The other three sightlines, with small equivalent widths, fall in-between the former and the latter in terms of volume density of galaxies. The three datapoints are all lying at higher volume density than the Bowen *et al.* points of similar equivalent width, but considering the small number statistics here it is probably not a significant offset. These galaxies all lie at smaller systemic velocities than those studied by Bowen *et al.* so it is possible that the neighborhoods of these local galaxies have been better surveyed. On the other hand these galaxies are so close ( $< 1500 \text{ km s}^{-1}$ ) that the estimation of the galaxy volume density by adding all galaxies within  $+500 \text{ km s}^{-1}$  and  $-500 \text{ km s}^{-1}$  probably does not make much sense considering the large deviations from a smooth Hubble Flow that are seen at these small distances from us.

While the choice of  $2 h^{-1}$  Mpc radius for estimating the galaxy volume density in Bowen *et al.* (2002) was rather arbitrary, the limiting  $M_B < -17.5$  was guided by the estimated completeness to  $B_{lim} = 15.5$  of the RC3 for the furthest targets of their sample. In our case because our galaxies are closer we can inspect the volume density down to a fainter limit using the RC3. In fact we know that our strongest line, for PG1309+355, is surrounded by dwarf galaxies in close proximity, but which were not counted in the previous volume density estimate because they were of lower magnitude than the  $M_{lim} < -17.5$ . For Figure 9 we have recomputed volume densities of galaxies down to  $M_{lim} < -16.5$ , which corresponds to

a  $B_{lim} = 15.5$  for our sample objects, and in a smaller cylinder of  $0.5 h^{-1}$  Mpc radius. Again the relation holds very well, although we are dealing with even smaller number statistics.

It thus appear that there is a relationship between the  $\text{Ly}\alpha$  column density along a sightline and the surrounding volume density of galaxies. This makes sense if the absorbers are simply part of the cosmic web. The galaxies have condensed in the densest parts of this network of filaments and sheets of gas, and hence the  $\text{Ly}\alpha$  detections will be denser when crossing a web filament/sheet rich in galaxies. The  $\text{Ly}\alpha$  absorbers are only detected within about  $< 170 h_{75}^{-1}$  kpc down to our limiting equivalent widths in the neighbourhood of galaxies because that is where the gas has higher column density in the filament, in the dense region from which the galaxy has condensed. On a larger scale, the  $\text{Ly}\alpha$  line will be stronger when crossing the core of a filament, or a busy 'intersection' of filaments of the web, where one finds a higher density of galaxy, on a scale of  $2 h^{-1}$  Mpc radius. That the relationship seems to still hold on the smaller scale of  $0.5 h^{-1}$  Mpc radius when considering the density of lower luminosity galaxies (Figure 9) is perhaps not surprising, as small groups of galaxies (like the agglomeration around PG1309+355) tend to be found on the periphery of larger clusters while most of our other targets are probably in semi-void regions (since galaxies were purposely selected to be isolated for the aim of this project). It is not obvious what should be the relevant scale to calculate the surrounding galaxy density. In simulations of the cosmic web, the filaments come in various thickness although are definitely of the order of the Mpc, down to the detectable column densities as here (Miralda-Escudé *et al.* 1996, Davé *et al.* 1999). Observations of double QSOs sightlines also find that, by looking at  $\text{Ly}\alpha$  lines in common in both spectra, the typical scale is around 0.5 Mpc (Dinshaw *et al.* 1997, 1998).

It is interesting to look also at the Doppler  $b$  parameters from the Voigt profile fits and compared them to those obtained by Bowen *et al.* (2002) (keeping in mind that some  $b$  values are uncertain because of the  $W - b$  degeneracy for saturated lines). In most of their sightlines several resolved  $\text{Ly}\alpha$  lines were added up (within their  $+500$  and  $-500 \text{ km s}^{-1}$  limit) to add up to the total equivalent widths plotted in Figure 8. In contrast, for most of our sample, the total equivalent widths come mostly from a single line. PG0804+761 is an exception, for which two lines were added, and also because the main line associated with the galaxy (ie. which matches more closely in velocity) is better fitted by two profiles rather than one. Similarly for PG1309+355, the profile, which has the highest equivalent width of all, is very broad and show several features, and the fit is considerably improved by fitting 3 voigt profiles rather than a single one. Interestingly the trend of Figure 8 holds well whether one is considering the addition of several narrow lines (typically  $b < 50 \text{ km s}^{-1}$ ) in the case of the Bowen *et al.* (2002) sample, or the denser, wider single  $b$  lines from our sample. One cannot exclude that our single lines are actually unresolved groups of narrower lines. If not there

might be a real physical difference in the density and temperature of the cosmic web gas depending on the environment, since our galaxies were mostly selected to be isolated, while the Bowen *et al.* (2002) ones are part of pairs or small groups. The Bowen *et al.* (2002) lines are also at redshifts on average twice as distant than for our sample. While some evolution with redshift is expected for the density of the cosmic web, since at lower redshift more of the gas will have condensed along the filaments (Davé *et al.* 1999), the two samples discussed here probably do not cover a wide enough range in redshift to see this. Our  $b$  values go up to about  $150 \text{ km s}^{-1}$ , unusually large for  $\text{Ly}\alpha$  forest absorption lines, although a few of the Bowen *et al.* (2002) sample do reach similar values. If the lines are indeed composed of only a single component, and assuming that the linewidth is purely due to the gas kinetic temperature (in which case  $b = \sqrt{2kT/m_p}$  with  $k$  being the Boltzmann constant and  $m_p$  the proton mass), then this would represent absorption from hot gas at a temperature of  $T = 60.6b^2$ , in our cases  $T = 0.4$  to  $1.4 \times 10^6 \text{ K}$ .

Based on these relationships it thus appears that the cosmic web is the most likely explanation for the origin of our  $\text{Ly}\alpha$  absorption-line detections. Thus the positive  $\text{Ly}\alpha$  detections, despite appearing in proximity to the target galaxies, are not directly related to these galactic disks, but only indirectly related because of the way that these galaxies are positioned in the large scale structure of the cosmic web.

## 5. Summary and Conclusions

Sightlines of QSOs at impact parameters 55 to  $387 h_{75}^{-1} \text{ kpc}$  from nine nearby galaxies (at systemic velocities from 566 to  $5538 \text{ km s}^{-1}$ ) were probed, using GHRS and STIS. In five cases a  $\text{Ly}\alpha$  absorption line was successfully detected at a velocity coincident with the galaxy's. Some of these  $\text{Ly}\alpha$  lines are the lowest-redshifts  $\text{Ly}\alpha$  lines ever detected, and in fact most of them are sitting on the wing of the Milky Way  $\text{Ly}\alpha$  damped line (hence introducing uncertainties in the derived equivalent widths). The positive detections occur for QSO-galaxy pairs with separations from 55 to  $169 h_{75}^{-1} \text{ kpc}$ , while non-detections are for pairs with separations from 162 to  $387 h_{75}^{-1} \text{ kpc}$ . Although at first sight it appears that the  $\text{Ly}\alpha$  lines might be genuinely arising in the extended disks of the target galaxies, this is not what transpires from inspecting the detailed kinematics of these galaxies. HI velocity fields were obtained at the VLA for our galaxies (and in one case was available from the literature), to derive their rotation curves. When comparing the inner rotation curves of the galaxies with the velocity at large radius provided by the  $\text{Ly}\alpha$  line it appears that it is very difficult to explain this  $\text{Ly}\alpha$  velocity as part of the extended gaseous rotating disk. In most cases one would need to invoke large warps in the extreme outer gas disks to reconcile the observed

velocities with the predicted ones. Worse, in some cases the Ly $\alpha$  line velocity indicates in fact counter-rotation with respect to the inner disk rotation.

In light of these results it appears that there is no detectable gas, down to levels of about  $10^{13} \text{ cm}^{-2}$ , corotating in an extended gaseous disk at radii  $> 35 \alpha^{-1}$ . The cosmic web is the most likely origin for the detected Ly $\alpha$  lines. The observed equivalent widths of the lines are consistent with this picture. Indeed the equivalent widths are correlated with the local volume density of galaxies around the sightline. This makes sense if the Ly $\alpha$  lines arise from the cosmic web, which is denser in regions of higher volume density of galaxies (since the galaxies have formed by condensating in the denser parts of the network). This correlation would be difficult to explain if the Ly $\alpha$  lines arised from halos or extended disks of the most nearby galaxy. One could argue that the equivalent widths should be larger for sighlines close to larger galaxies, which tend to be found in regions of higher galaxy volume density, which could then explain the trend observed. However if this were the case then one would observe presumably an even stronger correlation between the equivalent widths and the luminosity of the nearby galaxy, and although this was reported to be the case by Chen *et al.* (1998) it is now clearly contested by the results of Bowen *et al.* (2002), as well as in our sample for which no correlation is found between equivalent widths and luminosities.

Note that these results do not necessarily imply that the dark matter haloes of these galaxies do not exist at the radii probed by our QSO sightlines. It simply means that there is no longer some detectable gas in rotation in an extended gas disk at these radii, and that the Ly $\alpha$  lines detected are due to foreground or background cosmic web gas surrounding the galaxy. In fact weak lensing studies seem to indicate that indeed the dark matter halo extend very far out, typically  $> 300 h_{75}^{-1} \text{ kpc}$  for a  $L_*$  galaxy (eg. the weak-lensing studies such as Smith *et al.* 2001). But there is no gas to trace its dynamics out there, at least down to our limiting column densities. HI as traced by background QSOs is therefore not a useful tracer of galactic potential in the far outer regions of a  $\sim 200 \text{ kpc}$  halo. Only weak lensing, and perhaps H $\alpha$  in recombination from the extended ionized disk (Bland-Hawthorn *et al.* 1997) are hopeful tracers of dynamics at such radii. These QSOs turn out however to be extremely useful to probe the phases of the cosmic web gas. Many more sightlines will be required though before one can attempt to understand the cosmic gas distribution and density, as well as its evolution with redshift. The planned HST COS spectrograph would have allowed to probe the sightlines of fainter QSOs which would greatly increase the available sample, and hopefully the decision regarding HST can be reversed in the future. Eventually the next generation of sensitive giant radio telescopes as the CLAR (Côté *et al.* 2002) and eventually the SKA, will be able to survey efficiently large areas of the sky down to colum densities as deep as  $10^{16} \text{ cm}^{-2}$ , and hence trace directly in emission the structure of such low column density gas in the cosmic web.

We wish to thank an anonymous referee for thorough comments that helped improve this manuscript. Ray Lucas and especially Jennifer Wilson are thanked for data reduction support during visits at STScI. SC thanks Jacqueline Bergeron for useful insights on QSO absorption lines. The National Radio Astronomy Observatory is a facility of the National Science Foundation operated under cooperative agreement by Associated Universities, Inc. This research has made use of the Canadian Astronomy Data Center, which is operated by the National Research Council of Canada's Herzberg Institute of Astrophysics. Extensive use of the NASA/IPAC Extragalactic Database (NED), operated by the Jet Propulsion Laboratory, California Institute of Technology, under contract with NASA, is acknowledged. The HIPASS data used here were obtained at the Parkes Telescope, part of the Australia Telescope funded by Australia for operation as a National Facility managed by CSIRO. Support for this work was provided by NASA through grant numbers GO-6665.02-95A and GO-07295.02-96A from the Space Telescope Science Institute, which is operated by AURA, Inc. under NASA contract NAS5-26555.

## REFERENCES

- Appleton, P.N., Foster, P.A., Davies, R.D. 1986, 221, 393
- Barcons, X., Lanzetta, K.M., Webb, J.K. 1995, *Nature*, 376, 321
- Barnes, D.G., Staveley-Smith, L., de Blok, W.J.G. et al 2001, *MNRAS*, 322, 486
- Begeman, K. 1987, Ph.D. thesis, Rijksuniversiteit Groningen
- Bland-Hawthorn, J., Freeman, K.C., Quinn, P.J. 1997, *ApJ*, 490, 143
- Bowen, D.V., Blades, J.C., Pettini, M. 1996, *ApJ*, 464, 141
- Bowen, D.V., Pettini, M., Blades, J.C. 2002, *ApJ*, 580, 169
- Carignan, C., Côté, S., Freeman, K.C., Quinn, P.J. 1997, *AJ*, 113, 1585
- Chen, H-W., Lanzetta, K.M., Webb, J.K., Barcons, X. 1998, *ApJ*, 498, 77
- Chen, H-W., Lanzetta, K.M., Webb, J.K., Barcons, X. 2001, *ApJ*, 559, 654
- Cohen, R.J. 1979, *MNRAS*, 187, 838
- Côté, S., Carignan, C., Freeman, K.C. 2000, *AJ*, 120, 3027

- Côté, S., Taylor, A.R., Dewdney, P.E. 2002, ASP Conference Series, eds Taylor, Landecker, Willis, vol.276, p.92
- Davé, R., Hernquist, L., Katz, N., Weinberg, D. H. 1999, ApJ, 511, 521
- de Vaucouleurs, G., de Vaucouleurs, A., Corwin, J.R. et al 1991, “Third reference catalogue of bright galaxies”, New York Springer Verlag (RC3)
- de Young, D.S., Heckman, T.M. 1994, ApJ, 431, 598
- Ebbets, D. 1995, “Calibrating HST: Post Servicing Mission”, eds A.Koratkar, C.Leitherer, p.207
- Dinshaw, N., Weymann, R.J., Impey, C.D. et al 1997, ApJ, 491, 45
- Dinshaw, N., Foltz, C.B., Impey, C.D., Weymann, R.J. 1998, ApJ, 494, 567
- Gibson, B.K., Giroux, M.L., Penton, S.V. et al 2001, AJ, 122, 3280
- Hartmann, D., Burton, W.B. 1997, “Atlas of galactic neutral hydrogen”, Cambridge University Press
- Hoffman, G.L., Lu, N.Y., Salpeter, E.E., Connell, B.M., Fromhold-Treu, R. 1998, ApJ, 500, 789
- Huchtmeier, W., Richter, O. 1989, “A General Catalog of HI observations of Galaxies”, New York Springer.
- Kerr, F.J., de Vaucouleurs, G. 1955, AuJPh, 8, 508
- Lanzetta, K.M., Bowen, D.V., Tytler, D., Webb, J.K. 1995, ApJ, 442, 538
- Lockman, F.J., Savage, B.D. 1995, ApJS, 97, 1
- McLin, K.M., Stocke, J.T., Weymann, R.J., Penton, S.V., Shull, J.M. 2002, ApJ, 574, L115
- Mac Low, M.M., McCray, R. 1988, ApJ, 324, 776
- Macri, L.M., Stetson, P.B., Bothun, G.D. et al 2001, ApJ, 559, 243
- Maloney, P. 1993, ApJ, 414, 41
- Meurer, G.R., Carignan, C., Beaulieu, S.F., Freeman, K.C. 1996, 111, 1551
- Miralda-Escudé, J., Cen, R., Ostriker, J.P., Rauch, M. 1996, ApJ, 471, 582

- Morris, S.L., Jannuzi, B.T., Weymann, R.J. 2002, ASP Conference Series, vol. 254, eds. J.S.Mulchaev & J.Stocke, p.72
- Nath, B.B., Trentham, N. 1997, MNRAS, 291, 505
- Navarro, J., Frenk, C., White, S.D.M. 1996, ApJ, 462, 563
- Penton, S.V., Stocke, J.T., Shull, J.M. 2002, ApJ, 5
- Persic, M., Salucci, P., Stel, F. 1996, MNRAS, 281, 27
- Rhee, M.H., van Albada, T.S. 1996, A&AS, 115, 407
- Richter, P., Savage, B.D., Wakker, B.P. et al 2001, ApJ, 549, 281
- Shapiro, P. & Field, G. 1976, ApJ, 205, 762
- Shull, J.M., Penton, S.V., Stocke, J.T. et al 1998, AJ, 116, 2094
- Shull, J.M., Giroux, M.L., Penton, S.V. et al 2000, ApJ, 538, L13
- Silk, J., Sunyaev, R.A. 1976, Nature, 260, 508
- Smith, D.R., Bernstein, G.M., Fischer, P., Jarvis, M. 2001, ApJ, 551, 643
- Steidel, C.C., Kollmeier, J.A., Shapley, A.E. et al 2002, ApJ, 570, 526
- Swaters, R.A., Sancisi, R. & van der Hulst, J.M. 1997, AJ, 491, 140
- Tripp, T.M., Lu, L., Savage, B.D. 1998, ApJ, 508, 200
- van Gorkom, J., Carilli, C., Stocke, J., Perlman, E. & Shull, J.M. 1996, AJ, 112, 1397
- van Gorkom, J.H. 1991, in "Atoms, Ions, and Molecules: New Results in Spectral Line Astrophysics", eds. Haschick and Ho, p.1
- Véron-Cetty, M., Véron, P. 1996, "A Catalogue of Quasars and Active Nuclei", ESO Scientific Report No.17
- Wakker, B.P. 1991, A&AS, 90, 495
- Wakker, B.P., Kalberla, P.M.W., van Woerden, H. et al 2001, ApJS, 136, 537

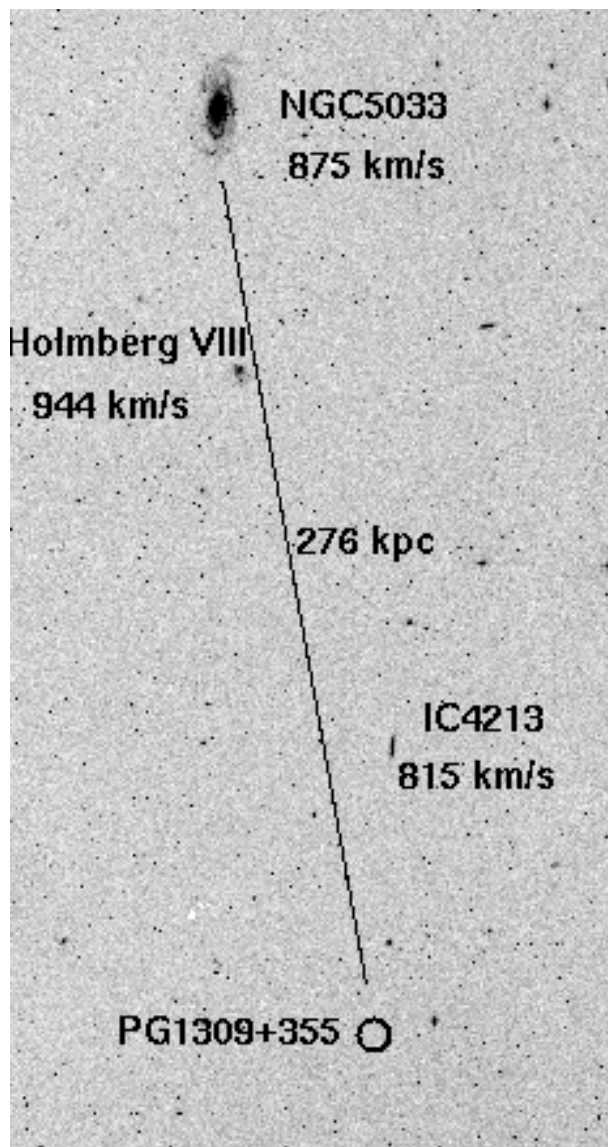


Fig. 1.— Digitized Sky Survey images (North up, East left) for our 5 galaxy-QSO pairs for which a  $\text{Ly}\alpha$  line was detected. The systemic velocity of the galaxy is indicated, as well as the projected distance to the QSO sightline. In the case of PG1309+355 there are also several dwarf galaxies close to the QSO sightline.



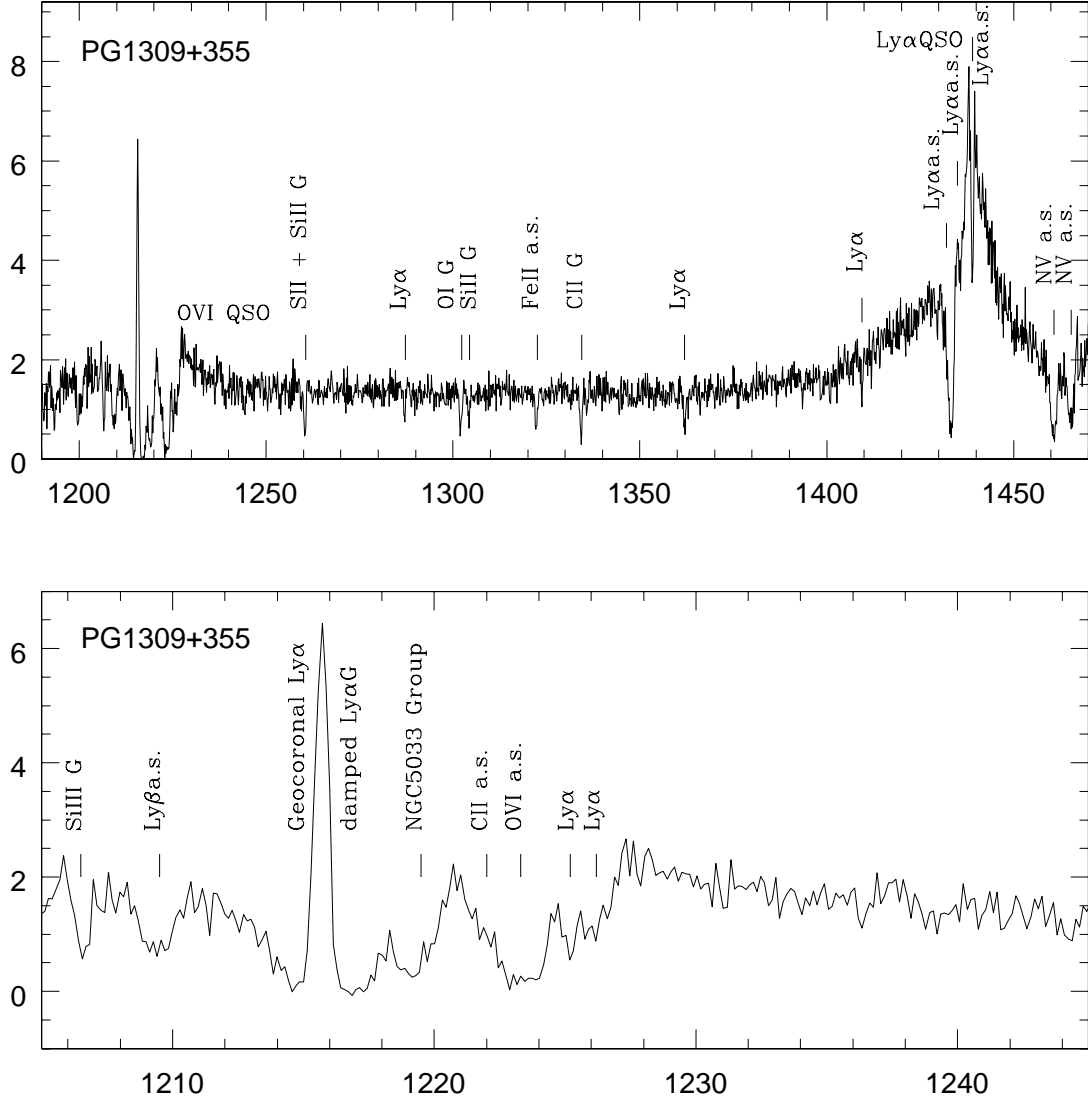
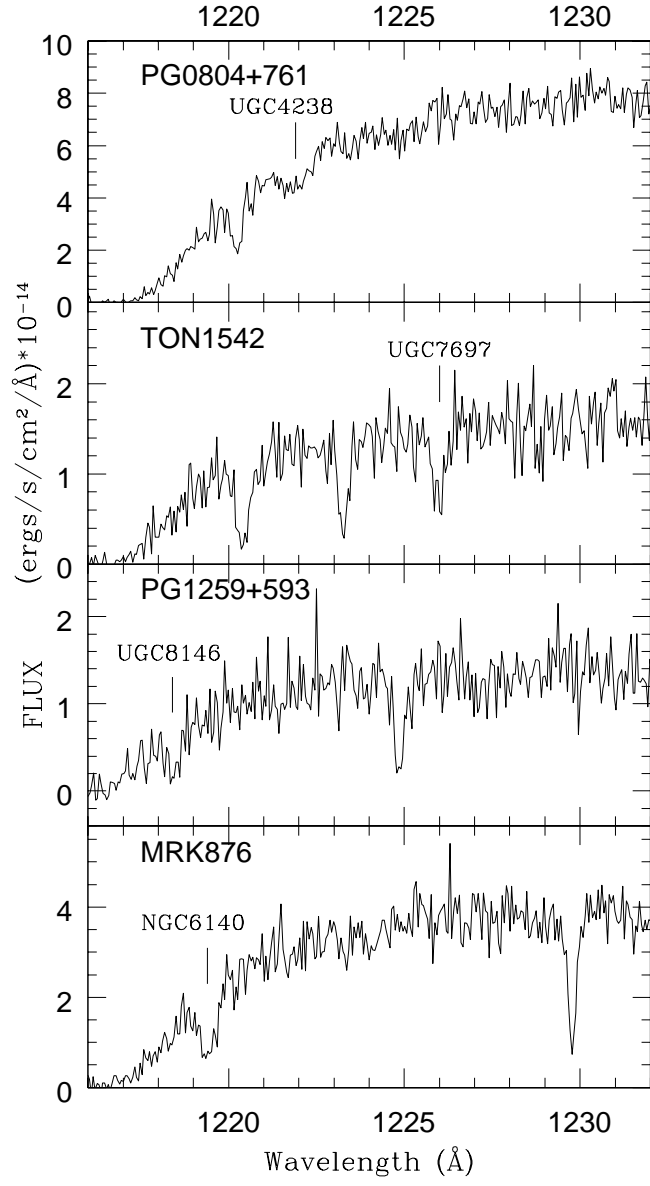
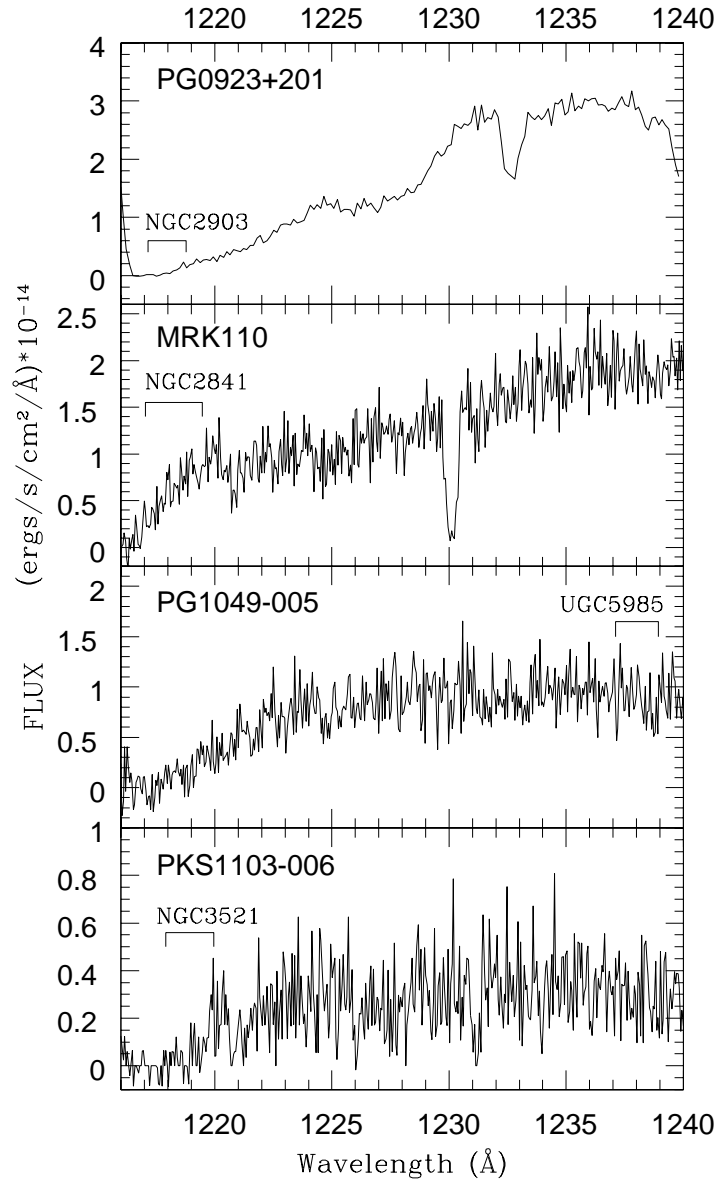


Fig. 2.— a) GHRs G160L spectrum of PG1309+355 and b) STIS G140M spectra for the other QSOs, with the detected Ly $\alpha$  absorption lines associated with our target galaxies. Lines indicated with "G" are galactic, those with "a.s." are from the associated absorption systems found around PG1309+355. Other Ly $\alpha$  lines are found at other various redshifts as well. c) Spectra of the QSOs with no detection of a Ly $\alpha$  absorption line associated with the target galaxy: GHRs G160L for PG0923+201 and STIS G140M for the others





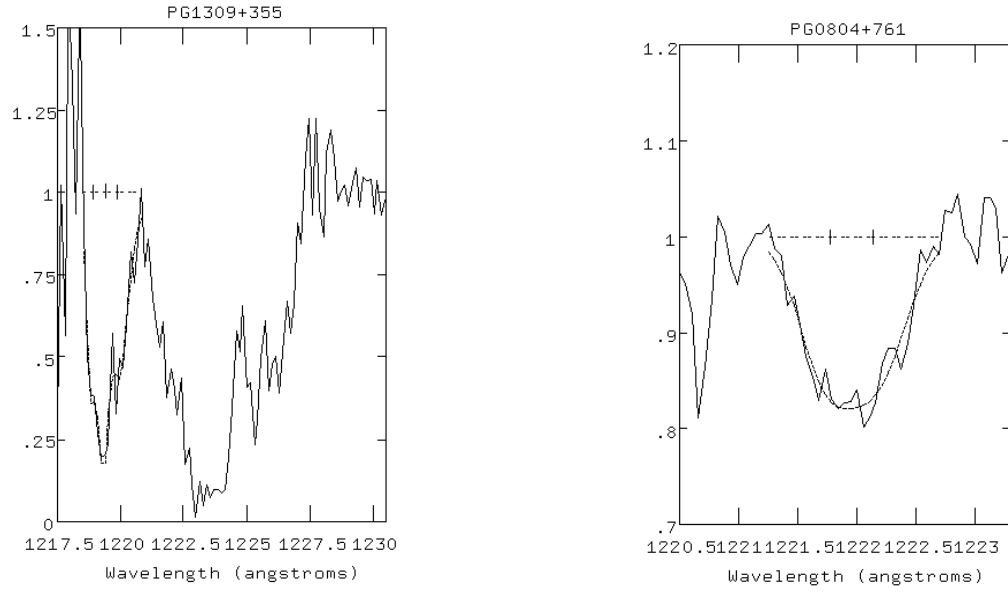
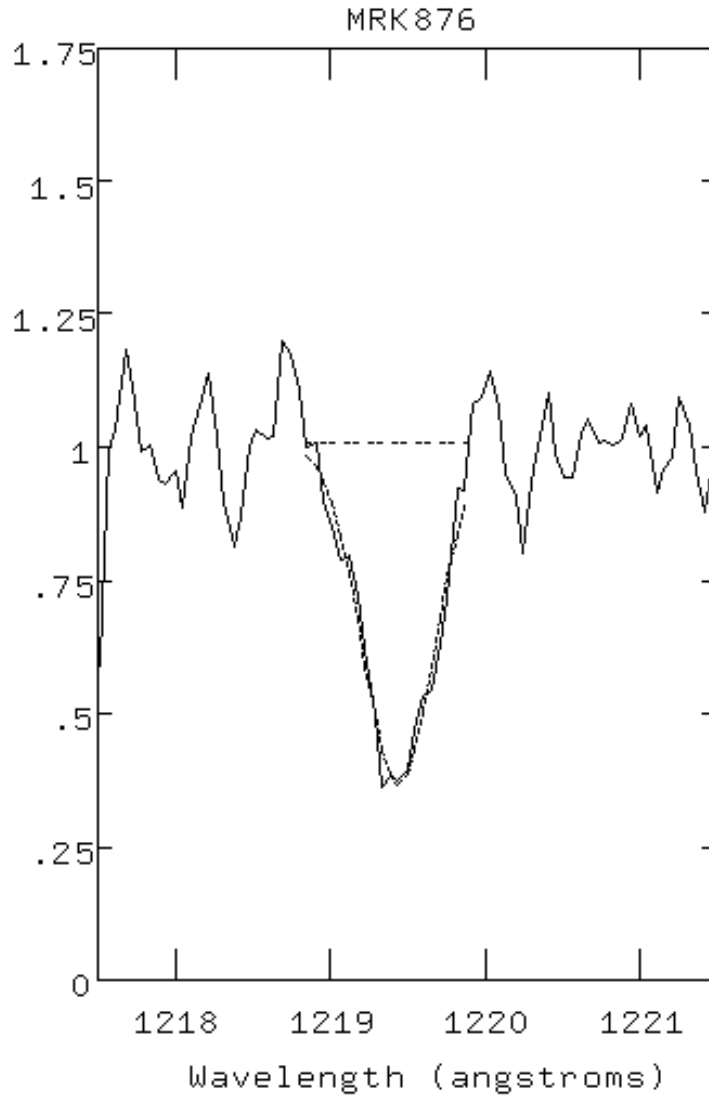
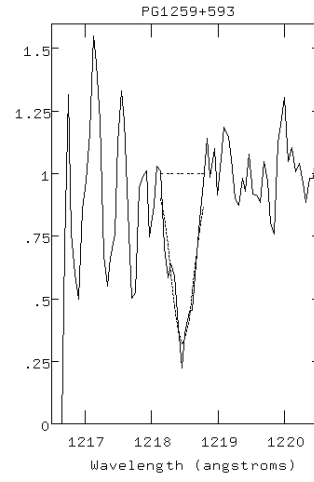
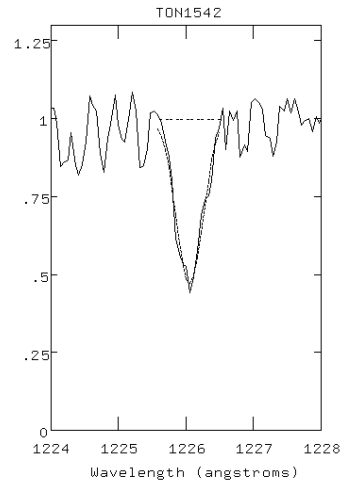


Fig. 3.— Normalized spectra with profile fits on the detected absorption lines (the subcomponents for PG1309+355 and PG0804+761 are shown as vertical ticks)



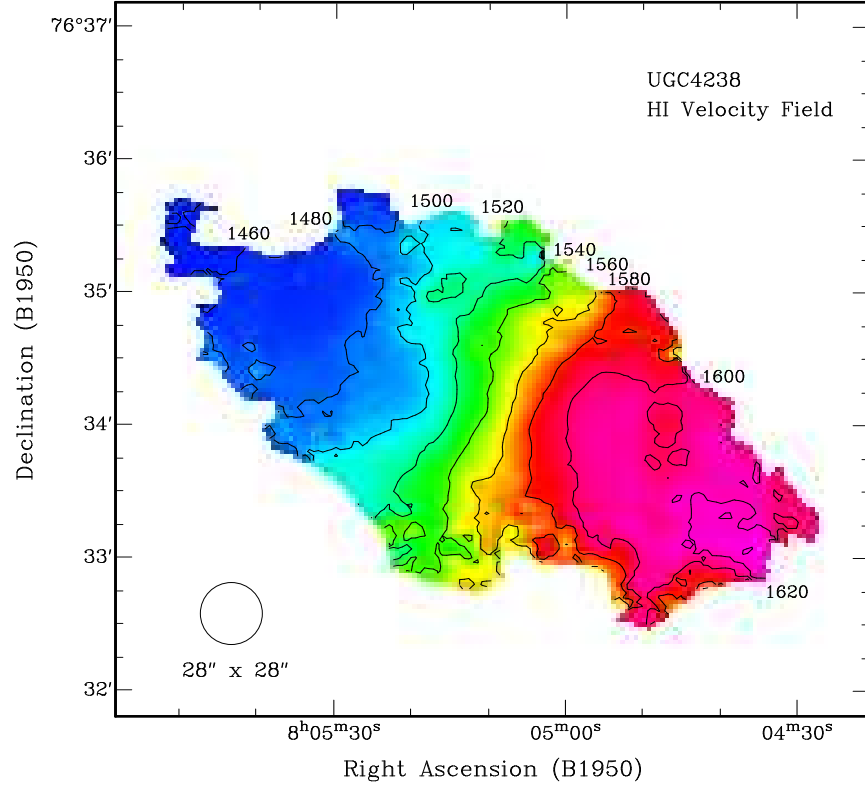
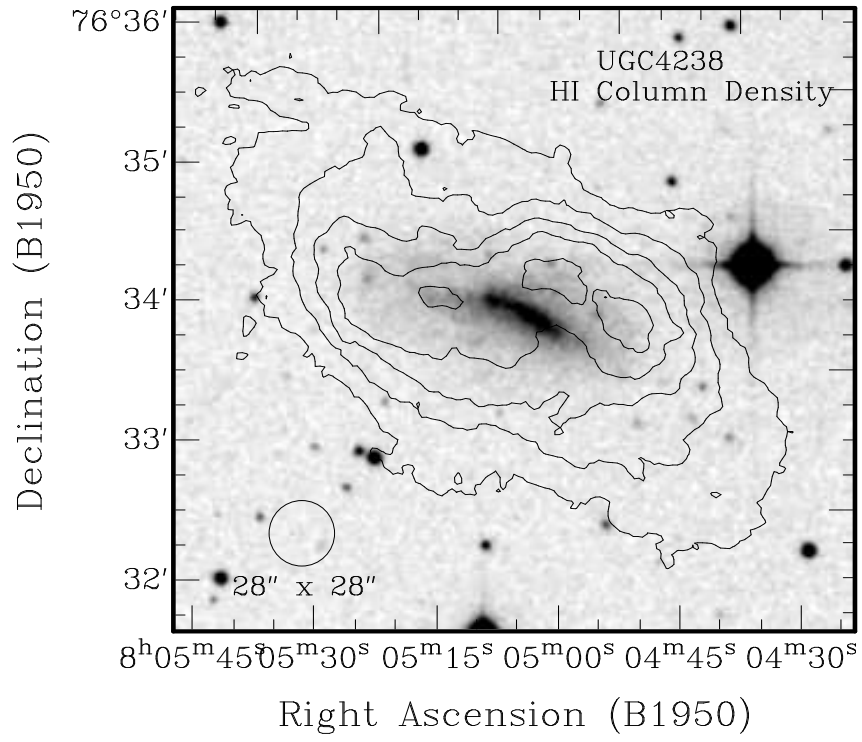
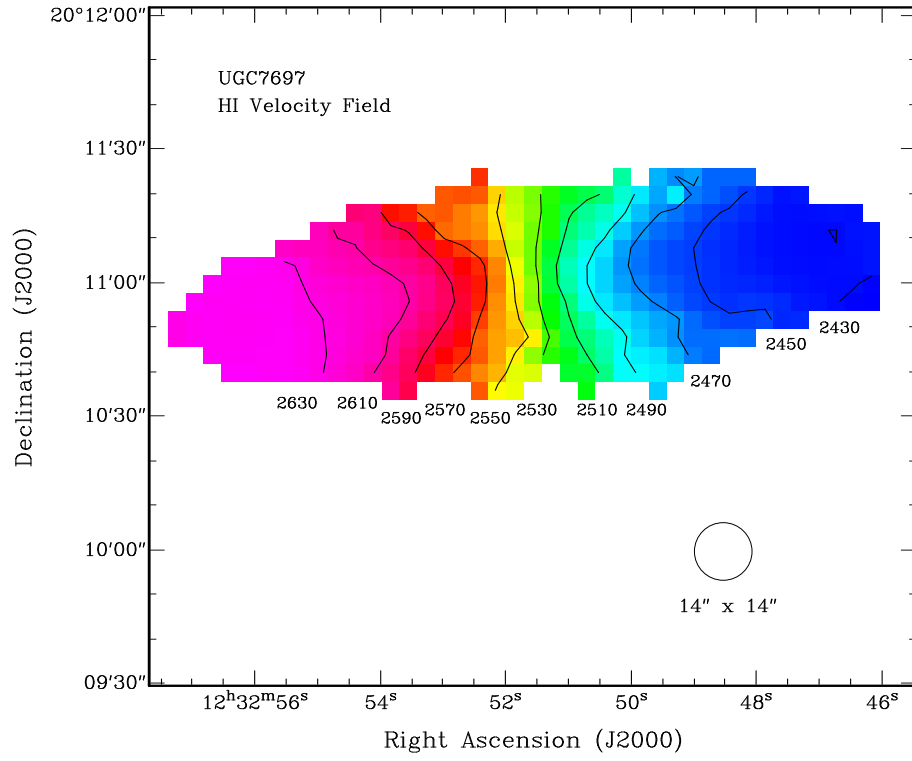
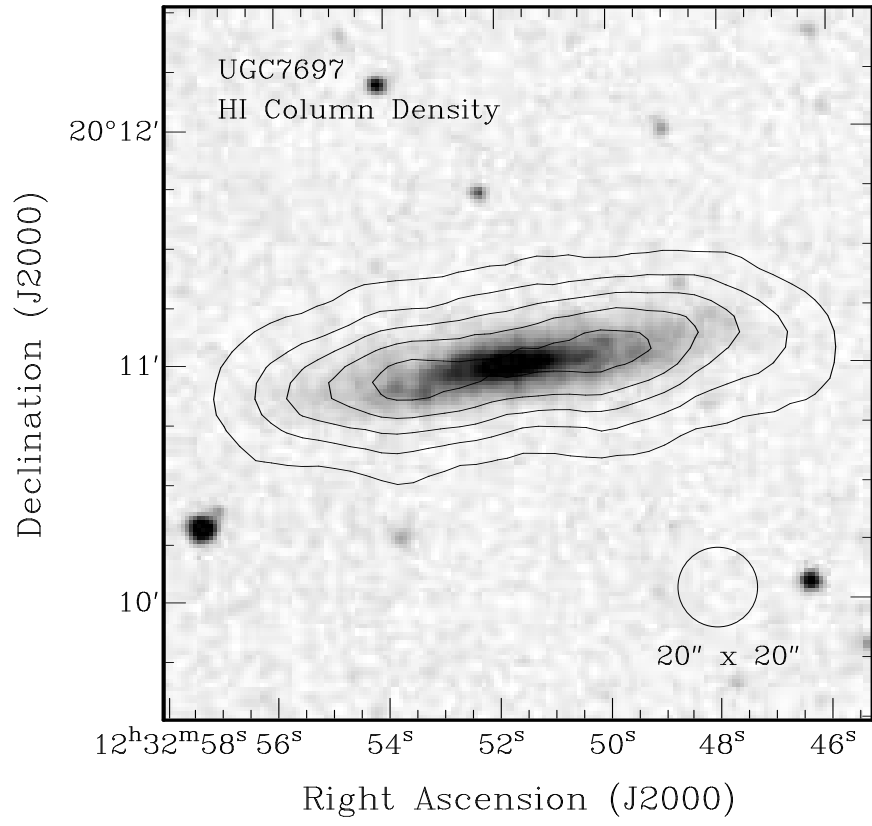


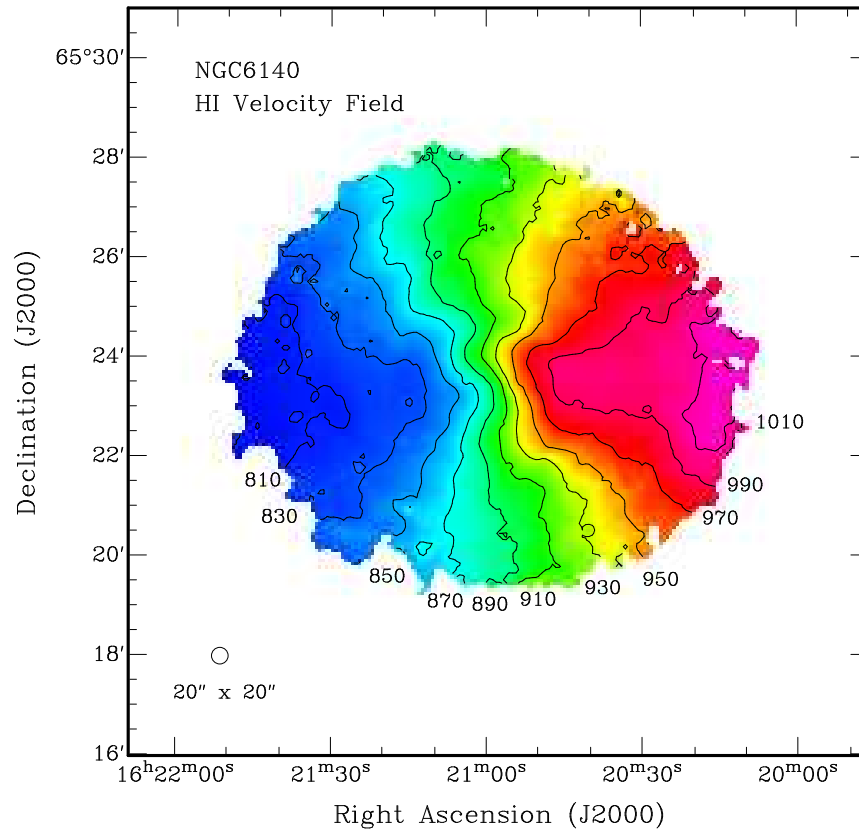
Fig. 4.— VLA HI velocity field and HI column density distribution over a DSS image, for UGC4238. The isovelocity contours are at interval of  $20 \text{ km s}^{-1}$ , and for the column density map the contour levels are at  $3.2, 9.5, 16.0, 22.0$  and  $28.4 \times 10^{20} \text{ atoms cm}^{-2}$ . Same for UGC7238, with contour levels at  $0.4, 1.3, 2.1, 3.0$  and  $3.8 \times 10^{20} \text{ atoms cm}^{-2}$ . Same for NGC6140, with contour levels at  $0.89, 2.7, 4.4, 6.2$  and  $8.0 \times 10^{20} \text{ atoms cm}^{-2}$ . The beam sizes are indicated in the lower corners of the figures.

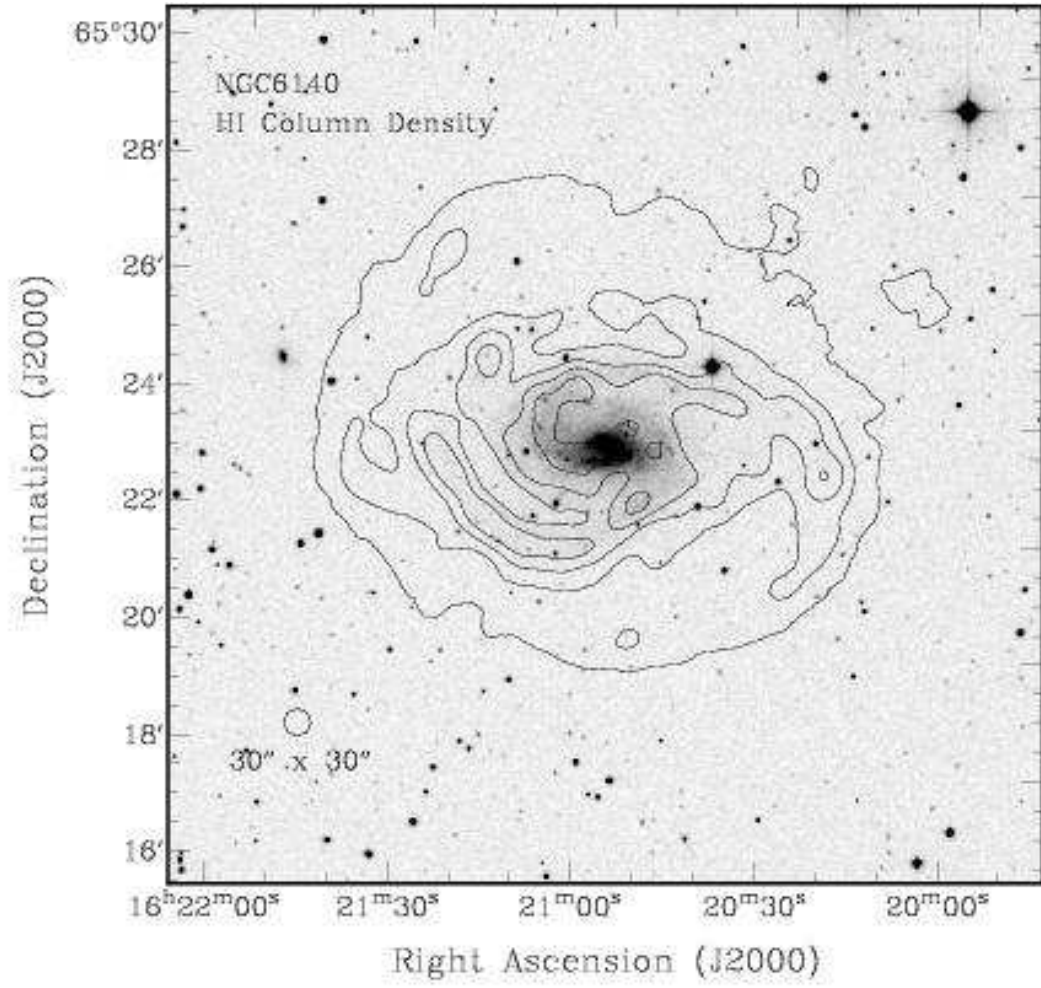












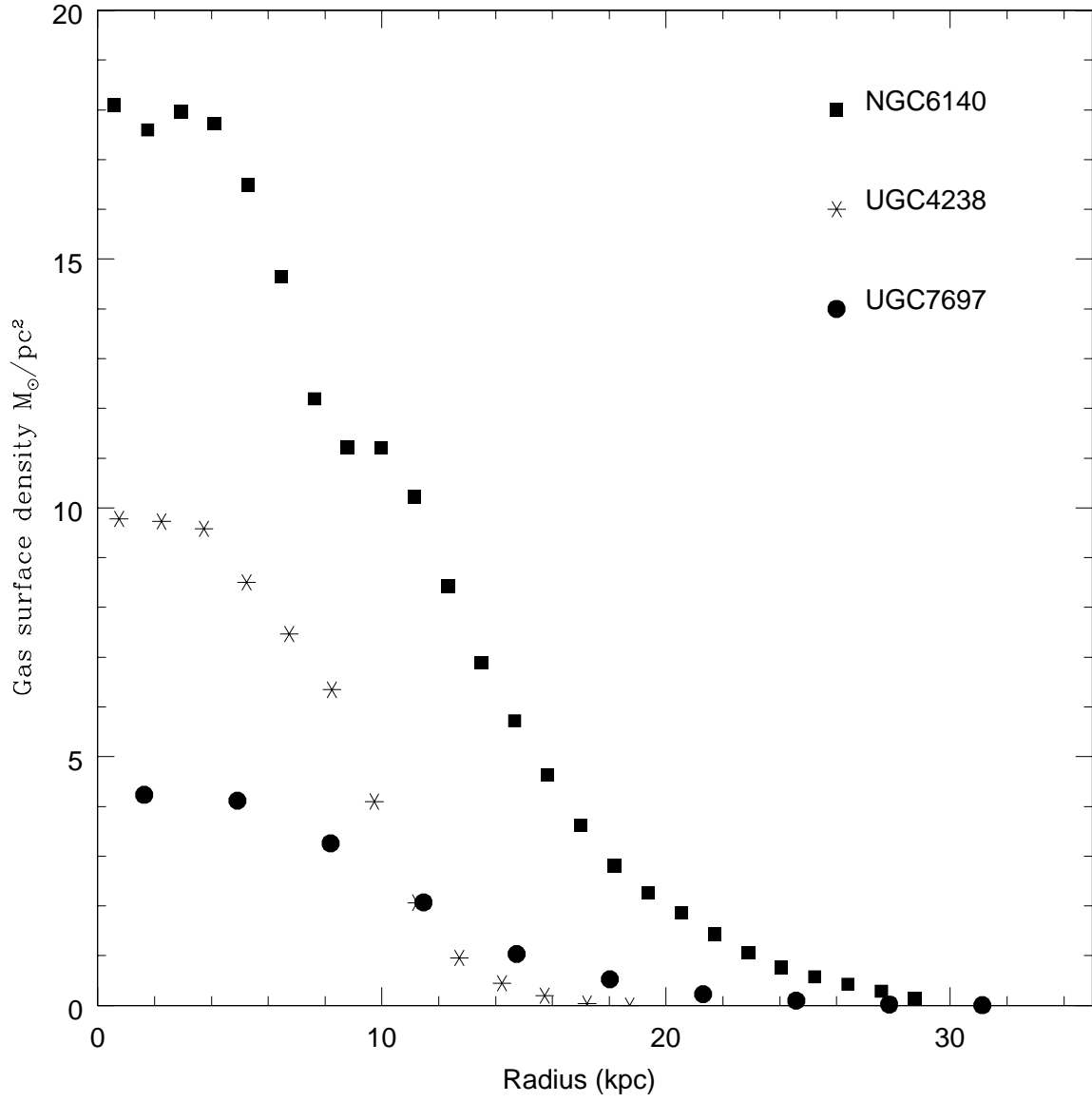


Fig. 5.— Gas radial surface density distributions for UGC4238, UGC7697 and NGC6140.

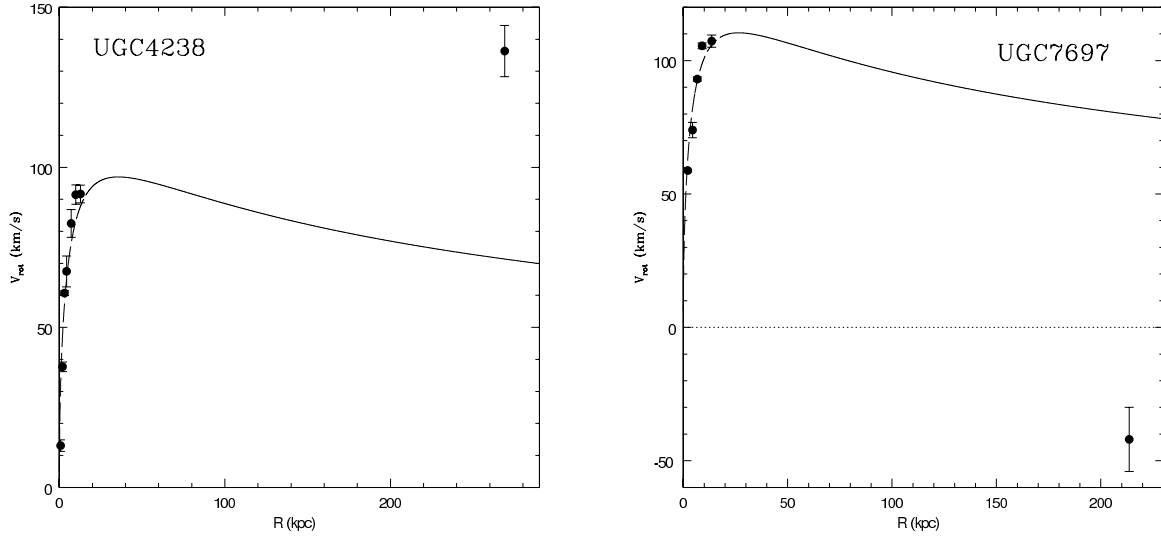
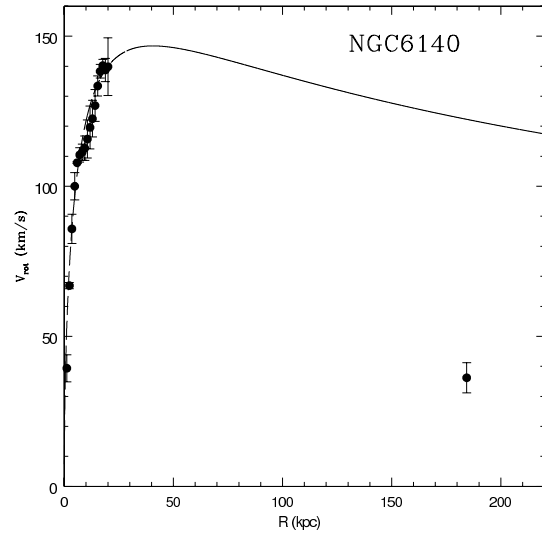
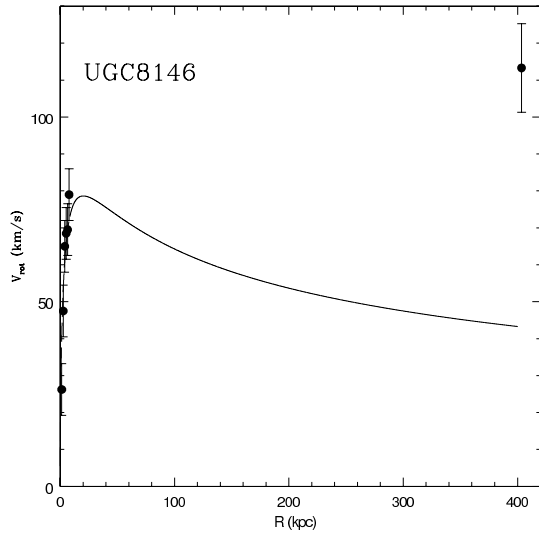


Fig. 6.— Rotation curves, consisting of HI velocities in the inner parts and the Ly $\alpha$  absorption line velocity at large radius. The line shows the velocities expected by CDM. The observed Ly $\alpha$  velocities do not agree with those expected for an extended corotating gaseous disk.



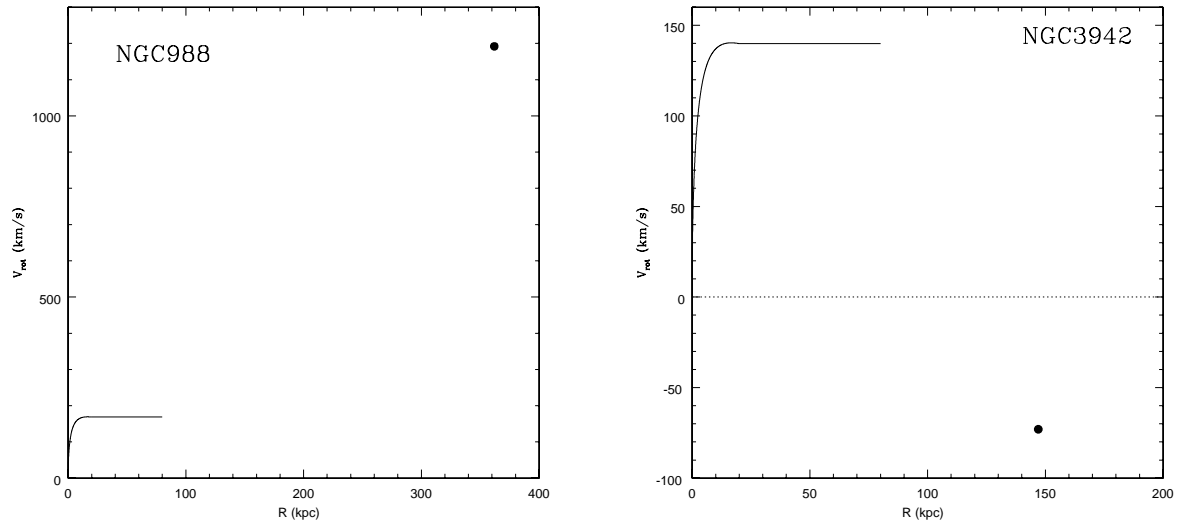


Fig. 7.— Same as Figure 5, for two galaxies from the Bowen *et al.* (2002) sample. No rotation curves are available for these galaxies so model ones based on the 'Universal Rotation Curve' of Persic & Salucci (1996) are used.

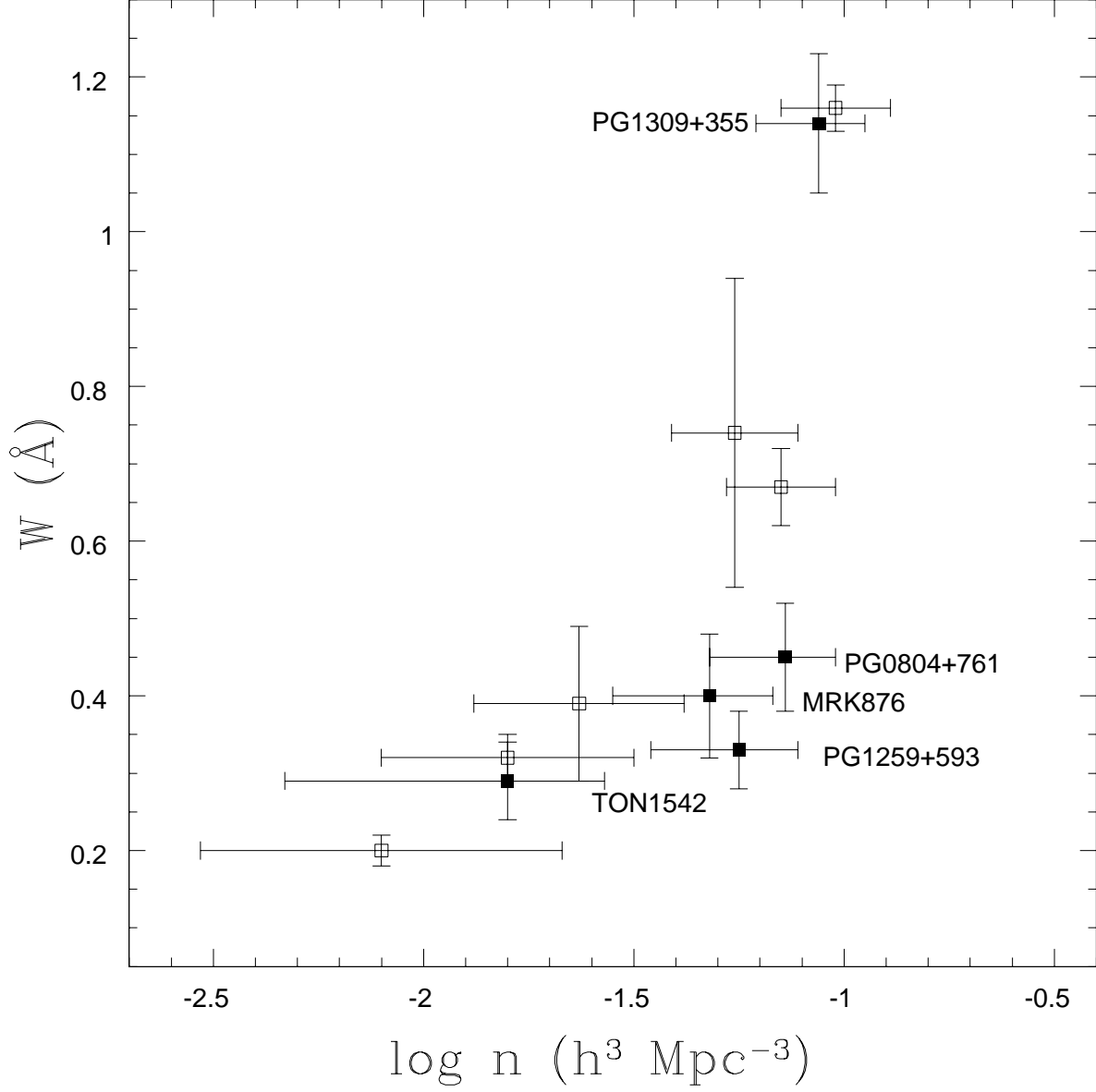


Fig. 8.— Total equivalent width versus the volume density of galaxies brighter than  $M_B = -17.5$  in a cylinder of radius  $2 h^{-1} \text{ Mpc}$  and length  $\pm 500 \text{ km s}^{-1}$  from the detected  $\text{Ly}\alpha$  line. Filled squares are for our sightlines, open ones for the sightlines of Bowen *et al.* (2002).



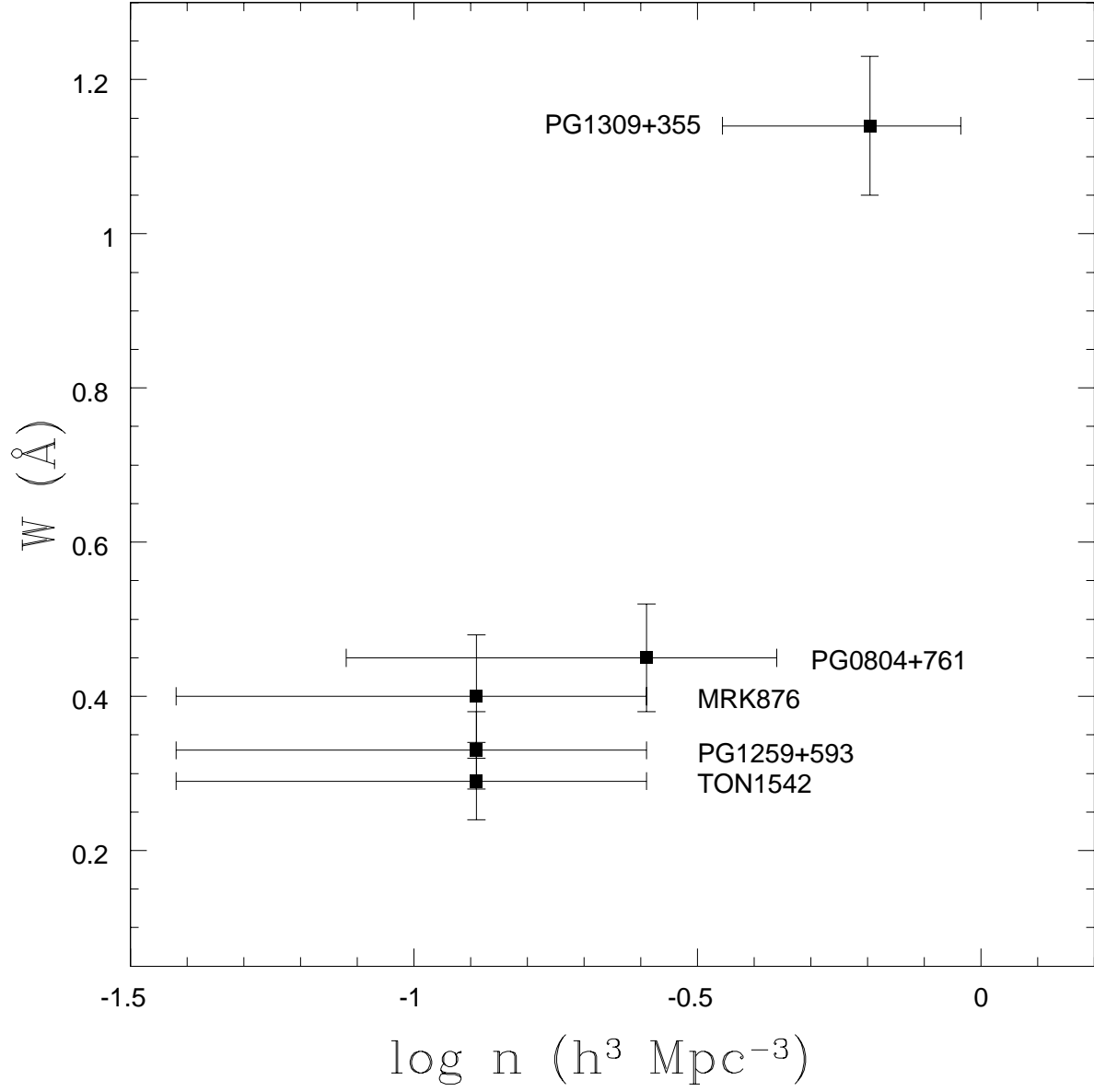


Fig. 9.— Same as Figure 7, for galaxies brighter than  $M_B = -16.5$  in a smaller cylinder of  $0.5 h^{-1} \text{ Mpc}$  and length  $\pm 500 \text{ km s}^{-1}$

Table 1. Details of the HST Observations (PID=6665 & 7295)

Object	RA (J2000)	Dec (J2000)	Redshift	Instrument	Dataset	Date	Exposure time (sec)
PG 0923+201	09:25:54.7	19:54:04	0.190	GHRS/G140L	z39r0106t	22/11/96	18550
PG 1309+355	13:12:17.7	35:15:21	0.184	GHRS/G140L	z39r0206m	26/07/96	2448
PG 0804+761	08:10:58.6	76:02:43	0.100	STIS/G140M	o4n301010	22/02/98	2448
MRK 110	09:25:12.9	52:17:11	0.035	STIS/G140M	o4n302010	20/05/99	2243
PG 1049-005	10:51:51.5	-00:51:18	0.3599	STIS/G140L	o4n303010	05/11/98	150
				STIS/G140M	o4n303020		1537
PKS 1103-006	11:06:31.7	-00:52:53	0.4233	STIS/G140L	o4n304010	08/04/99	190
				STIS/G140M	o4n304020	08/04/99	1440
TON 1542	12:32:03.6	20:09:29	0.064	STIS/G140M	o4n305010	29/05/99	1990
PG 1259+593	13:01:12.9	59:02:07	0.4778	STIS/G140L	o4n307010	26/03/99	120
				STIS/G140M	o4n307020		1808
MRK 876	16:13:57.2	65:43:09	0.129	STIS/G140M	o4n308010	19/09/98	2298

Table 2. Target QSO-galaxies parameters and results

QSO	Galaxy	Type	$M_B^a$	Distance <sup>b</sup> (Mpc)	$\rho^c$ (arcmin) (kpc)	$\rho/D_{25}^d$	$V_{gal}^e$ (km s <sup>-1</sup> )	$V_{Ly\alpha}^f$ (km s <sup>-1</sup> )	$W^g$ (Å)	$b^h$ (km s <sup>-1</sup> )	$\log N_{HI}^i$ (cm <sup>-2</sup> )
PG 0923+201	NGC 2903	SB(s)d	-20.3	7.6	130.1 287	10.3	566	-	< 0.14	-	-
PG 1309+355	NGC 5033 Group	SA(s)c	-20.1	11.7	81.5 276	7.6	875	876.9 ± 18	1.10 ± 0.17	87, 147, 153	13.6, 14.0, 14.0
PG 0804+761	UGC 4238	SBd	-18.7	20.6	22.7 136	9.5	1544	1569.9 ± 8	0.26 ± 0.03	131, 141	13.2, 13.2
MRK 110	NGC 2841	SA(r)b	-21.2	14.1	84.0 344	10.4 <sup>j</sup>	638	-	< 0.09	-	-
PG 1049-005	UGC 5985	S0/a	-21.0	73.8	18.1 387	9.5	5538	-	< 0.08	-	-
PKS 1103-006	NGC 3521	SAB(rs)bc	-20.9	10.7	51.9 162	4.7	805	-	< 0.22	-	-
TON 1542	UGC 7697	Scd	-18.9	33.8	11.4 112	5.4	2536	2556.9 ± 12	0.29 ± 0.07	104	13.73
PG 1259+593	UGC 8146	Scd	-16.7	8.9	21.3 55	6.1	669	679 ± 12	0.33 ± 0.08	109	13.78
MRK 876	NGC 6140	SB(s)cd	-18.8	12.1	47.8 169	7.6	910	935 ± 5	0.39 ± 0.07	131	13.87

<sup>a</sup>Blue absolute magnitude of the galaxy, corrected for Galactic and internal absorption, from the RC3.

<sup>b</sup>Calculated using  $H_0=75$  km/s/Mpc, except NGC2841 which has a Cepheid distance.

<sup>c</sup>Impact parameter between the QSO sightline and the center of the galaxy, in arcmin and in kpc

<sup>d</sup>Ratio of the impact parameter to the optical diameter of the galaxy, measured at a surface brightness level of 25 mag/arc<sup>2</sup>

<sup>e</sup>Heliocentric velocity of the galaxy

<sup>f</sup>Heliocentric velocity of the Ly $\alpha$  absorption. In the case of PG 1309+355 where the line is better fitted by three components, the corresponding velocities are  $v_1=714.7$ ,  $v_2=840.4$  and  $v_3=1016.0$  km s<sup>-1</sup>. Similarly for PG 0804+761 the two components have  $v_1=1506.0$  and  $v_2=1614.5$  km s<sup>-1</sup>.

<sup>g</sup>Total equivalent width or  $3\sigma$  detection limit in case of non-detection

<sup>h</sup>Doppler  $b$  parameter of the line or different components of the line

<sup>i</sup>HI column densities

<sup>j</sup>There is another galaxy close to this sightline, UGC5047, at  $cz=507$  km/s. However it is a small dwarf and although it is only  $108 h_{75}^{-1}$  kpc away, its  $\rho/D_{25}$  is over 35.

Table 3. Observing log for the VLA data and HI properties

Source	Date	Array	$t_{int}$ (hours)	Central Velocity ( $\text{km s}^{-1}$ )	Beam <sup>a</sup>	rms <sup>b</sup> ( $\text{mJy beam}^{-1}$ )	$V_{sys}$ <sup>c</sup> ( $\text{km s}^{-1}$ )	$\langle PA \rangle$ <sup>d</sup> ( $^{\circ}$ )	$\langle i \rangle$ <sup>e</sup> ( $^{\circ}$ )	$M_{HI}$ <sup>f</sup> $10^9 M_{\odot}$	$D_{HI}$ <sup>g</sup> (arcmin)
UGC4238	Nov 8, 1998	VLA B/C	1.5	1560	$12'' \times 12''$	2.4	1544	255	62	2.27	5.0
UGC7697	Apr 17, 2000	VLA C	4.6	2540	$14'' \times 14''$	1.0	2535	99	80	1.69	2.5
NGC6140	Apr 21, 2000	VLA C	4.3	910	$14'' \times 14''$	1.2	911	276	49	3.51	9.3

<sup>a</sup>Resulting beam size, full resolution (uniform weighting)

<sup>b</sup>rms noise in channel maps at full resolution after Cleaning

<sup>c</sup>Systemic (heliocentric) velocity of the galaxy

<sup>d</sup>Average Position Angle of the HI distribution

<sup>e</sup>Average Inclination of the HI distribution

<sup>f</sup>Total Mass of HI, at the adopted distances listed in Table 2

<sup>g</sup>HI diameter, at the  $1 M_{\odot} \text{pc}^{-2}$  level

Table 4: Rotation Curves

Galaxy	Radius (kpc)	Velocity ( $\text{km s}^{-1}$ )	Error ( $\text{km s}^{-1}$ )
UGC4238	0.798	13.07	1.79
	1.995	37.7	1.49
	3.19	60.7	0.76
	4.389	67.5	4.82
	7.183	82.48	4.36
	9.98	91.46	3.03
	12.77	91.67	2.8
UGC7697	2.13	58.77	0.52
	4.42	73.99	2.87
	6.72	93.10	0.82
	9.01	105.52	1.07
	13.60	107.3	2.25
NGC6140	1.18	39.36	4.5
	2.35	66.93	1.05
	3.53	85.80	4.87
	4.81	100.03	4.54
	5.88	107.86	0.29
	7.06	110.48	2.4
	8.24	111.39	2.68
	9.41	112.69	4.04
	10.59	115.74	6.34
	11.77	119.60	7.11
	12.95	122.53	6.11
	14.12	126.91	5.30
	15.3	133.43	3.33
	16.48	138.31	2.28
	17.65	140.21	2.05
	18.83	138.75	3.89
	20.01	139.85	9.63